A nanobody activating metabotropic glutamate receptor 4 discriminates between homo- and heterodimers

Jordi Haubrich, Joan Font, Robert Quast, Anne Goupil-Lamy, Pauline Scholler, Damien Nevoltris, Francine Acher, Patrick Chames, Philippe Rondard, Laurent Prézeau, et al.

A nanobody activating metabotropic glutamate receptor 4 discriminates between homo and heterodimers

Jordi Haubrich[a,1], Joan Font[a,1], Robert B. Quast[b], Anne Goupil-Lamy[c], Pauline Scholler[a], Damien Nevoltris[d], Francine Acher[e], Patrick Chames[d], Philippe Rondard[a], Laurent Prézeau[a,*] & Jean-Philippe Pin[a,*]

[a]*Institut de Génomique Fonctionnelle, University of Montpellier, CNRS, INSERM, 34094 Montpellier Cedex 5, France;* [b]*Centre de Biologie Structurale (CBS), University of Montpellier, CNRS, INSERM, 34090 Montpellier, France* ; [c]*BIOVIA, Dassault Systèmes, F-78140, Vélizy-Villacoublay Cedex, France;* [d]*Institut Paoli-Calmettes, Aix Marseille University, CNRS, INSERM, CRCM, 13009 Marseille, France;* [e]*Faculté des Sciences Fondamentales et Biomédicales, Université de Paris, CNRS, 75270 Paris Cedex 06, France.*

Author contributions: J.H., J.F., F.A., P.C., L.P. and J.-P.P. designed research; D.N. generated and screened nanobodies; J.H., J.F., A.G., F.A. and P.S. performed research; J.H., J.F., F.A., and P.S. analyzed data; R.Q. performed single-molecule FRET research and analysis; and J.H., J.F., F.A., P.R. and J.-P.P. wrote the paper.

[1]J.H. and J.F. contributed equally to this work.

[*]To whom correspondence may be addressed. Email: laurent.prezeau@igf.cnrs.fr or jean-philippe.pin@igf.cnrs.fr.

Classification: Biological Sciences, Pharmacology

Keywords: G protein-coupled receptor | single domain antibody | activation mechanism | agonist | allosteric regulation | epitope mapping | molecular modelling

Abstract

There is growing interest in developing biologics due to their high target selectivity. The G protein-coupled homo and heterodimeric metabotropic glutamate (mGlu) receptors regulate many synapses and are promising targets for the treatment of numerous brain diseases. Although subtype selective allosteric small molecules have been reported, their effects on the recently discovered heterodimeric receptors are often not known. Here we describe a nanobody that specifically and fully activates homodimeric human mGlu4 receptors. Molecular modelling and mutagenesis studies revealed that the nanobody acts by stabilizing the closed active state of the glutamate binding domain by interacting with both lobes. In contrast, this nanobody does not activate the heterodimeric mGlu2-4, but acts as a pure positive allosteric modulator. These data further reveal how an antibody can fully activate a class C receptor and bring further evidence that nanobodies represent an alternative way to specifically control mGlu receptor subtypes.

Significance statement

Biologics, and especially antibodies are promising therapeutics. Antibodies are expected to show higher subtype selectivity and less off-target activity than small molecules. GPCRs being the main drug targets, there is a need for antibodies modulating these receptors. Here we describe the first single domain antibody fully activating a GPCR. This nanobody activates the homodimeric metabotropic glutamate receptor type 4 (mGlu4), an interesting target for the treatment of Parkinson's disease or pain. Using modeling tools, we show this nanobody acts by

stabilizing the active form of the binding domain. It does not activate heterodimeric mGlu receptors containing the mGlu4 subunit. These data revealed that nanobodies can be instrumental tools to specifically control mGlu receptor subtypes.

Introduction

There is more and more interest in developing antibodies as possible pharmacological and even therapeutic agents (1, 2). The single domain antibodies, also named nanobodies, are prone for such activities as their short variable loops can interact in surface cavities that can vary between the conformational states of a protein (1). As such, nanobodies regulating drug targets have already been reported (3, 4). Among the main drug targets are the G protein-coupled receptors (GPCRs) that play important roles in cell-cell communication (5).

Among the large GPCR family, class C receptors are those activated by the main neurotransmitters, glutamate and γ-amino butyric acid (GABA), as well as by Ca^{2+} ions, sweet and umami compounds (6). There are eight genes encoding metabotropic glutamate (mGlu) receptor subunits. Although only considered as disulfide linked homodimers, the complexity of the mGlu receptor family increased with the description of heterodimeric entities made of two different mGlu subunits (7). Indeed, the post-synaptic mGlu1 and 5 on one side, and pre-synaptic mGlu2, 3, 4, 7 and 8 subunits on another side can form heterodimeric entities in recombinant cells, leading to the possible existence of 16 additional mGlu subtypes (7, 8). Among these, the mGlu2-4 heterodimer retained much attention. It was found to display a specific pharmacological profile and was identified in transfected neurons, as well as in both cortico-striatal (9) and lateral perforant path (10) terminals. Identifying the

various heterodimeric mGlu receptors in the brain and their possible roles is essential.

We recently reported nanobodies acting as positive allosteric modulators (PAMs) specific to the mGlu2 homodimer (11). Among the mGlu subtypes, the mGlu4 containing receptors, and especially mGlu4 homodimers, are of interest for the treatment of Parkinson disease (12–14) and pain (15, 16). In the present study, we report the identification of DN45, a nanobody that specifically and fully activates human mGlu4 homodimers. We show that this nanobody acts by stabilizing the closed active state of the glutamate binding Venus flytrap domain (VFT). However, this nanobody was unable to directly activate the mGlu2-4 heterodimer, acting instead as a pure PAM. These data reveal a novel way a nanobody can activate a class C GPCR, and confirm the potential of using nanobodies to discriminate between homo- and heterodimeric receptors.

Results

DN45 is specific to the human mGlu4 receptor

To identify nanobodies targeting mGlu4, HEK293 cells transiently expressing either the human or the rat mGlu4 receptor were injected in a llama. Genes encoding V_HH domains were amplified by reverse transcription polymerase chain reaction (RT-PCR) from the total RNA of peripheral blood mononuclear cells and used to create a phage display library. This library was depleted on controlled HEK293 cells and enriched by two cycles of positive selection on human mGlu4 transfected cells in the presence of an excess of anti-HEK293 nanobodies (17). Nanobody containing *E. coli* supernatants were screened by flow cytometry.

Among the selected clones, nanobody DN45 was further characterized. We performed a binding assay based on time-resolved fluorescence energy transfer (TR-FRET) between the SNAP-tagged receptor and an anti-c-Myc-antibody-d2 interacting with the c-Myc-tag inserted at the C terminal end of the DN45 sequence (Fig. 1A). The nanobody binds to human mGlu4 exclusively when tested at 100 nM and no binding was observed on any other human mGlu receptor (Fig. 1B), nor on the eight rat mGlu receptors (Fig. 1C). To avoid constitutive receptor activation by ambient glutamate produced by the cultured HEK293 cells, excitatory amino acid transporter 3 (EAAC1) was co-transfected with the indicated receptors, such that receptors were essentially in an inactive state under basal condition. Activating any of the mGlu receptors with an agonist did not allow binding of DN45 either, except on the human mGlu4 where a higher signal was observed (Fig. 1B, C). Indeed, DN45 had a preferred high binding affinity (K_D = 3.1 nM) for the active conformation of the human mGlu4 receptor and a low binding affinity for the basal and antagonist-induced conformation (Fig. 1D and *SI Appendix*, Table S1).

DN45 is a full agonist of the mGlu4 receptor

In agreement with the higher binding affinity of DN45 for the active form of hmGlu4 receptor, DN45 alone stabilizes the active conformation of the VFT dimer as revealed using a TR-FRET based conformational biosensor (Fig. 2A) (7, 18). This biosensor measures the distance variation between the N-terminally inserted SNAP tags of the subunits, such that a high TR-FRET is measured in the basal state (after random labelling with the SNAP substrates O^6-benzylguanine (BG)-Lumi4-Tb and BG-Green), while a lower TR-FRET is observed upon the reorientation of the VFTs upon activation (18). DN45 displays a potency, and efficacy not significantly different from the group-III mGlu receptor agonist L-AP4 (Fig. 2A and *SI Appendix*, Table S2). Subsequently, we setup a single-molecule FRET (smFRET) approach to compare the agonist effect of L-AP4 and DN45 at the single-molecule level in an environment without ambient glutamate (Fig. 2B and *SI Appendix*, Fig. S1, Table S3). There was no difference between the apo-state and the antagonist-stabilized state. However, both L-AP4 and DN45 acted as full agonists as illustrated by the similar increase in the proportion of molecules in the low FRET, active conformation. DN45 also activated the natural Gi protein of the mGlu4 receptor with the same potency as L-AP4, as revealed with a Gi bioluminescence resonance energy transfer (BRET) sensor (Fig. 2C and *SI Appendix*, Fig. S2, Table S2). The agonist activity of DN45 was further confirmed by measuring the accumulation of IP-1 upon activation of the chimeric G protein Gqi9 (Fig. 2D). DN45 potency and efficacy were similar to those obtained with L-AP4, both being more potent than glutamate (Fig. 2D and *SI Appendix*, Table S2). In presence of high concentrations of LY341495, the potency of DN45 was decreased (Fig. 2E). Of note, the L-AP4 potency for accumulation of IP-1

was not significantly increased in the presence of non-saturating DN45 concentrations (Fig. 2F and *SI Appendix*, Table S2).

Residues in lobe 2 of the human mGlu4 VFT confer subtype selectivity to DN45

To explain the subtype selectivity of DN45, we substituted any individual residue at the surface of the human mGlu4 VFT into its rat equivalent. We identified twelve residues on the surface of the VFT that are different in the human and rat proteins (Fig. 3A). Among the twelve mutations tested, three (i.e. I318S, H323R and D485G) affected DN45 binding, with D485G suppressing binding completely (Fig. 3B). Consistent with these binding data, the DN45 agonist effect was largely affected or even suppressed in these human mGlu4 mutants (Fig. 3C), while L-AP4 could still activate them (*SI Appendix*, Fig. S3A).

Molecular modelling identifies DN45-mGlu4 interaction site on both lobe 2 and lobe 1

We built 3D models of both human mGlu4 (in an active closed conformation) and DN45, and performed docking experiments using ZDOCK (19) without any specific constraint. Our best scored model using ZRANK (20), that keeps the main interactions with or without L-AP4 within the VFT binding site after a 10 ns dynamics simulation, revealed possible interaction sites of DN45 on the VFT (Fig. 3A). In the presence of bound L-AP4, more interactions between the partners were detected (*SI Appendix,* Fig. S4A, B) in agreement with the higher binding affinity in the active state. A time-dependent analysis of the model revealed the mGlu4 residues maintaining interaction with DN45 during the 10 ns molecular dynamics simulations (*SI Appendix,* Fig. S5). These include the residues that are human-specific: I318, H323, D485 (lobe 2) and also residues on lobe 1 (*SI Appendix,* Fig. S5). The virtual

mutagenesis analysis performed on our 3D model of the mGlu4-DN45 complex is perfectly in line with the evaluated impact of individually substituting the twelve human-specific residues for its rat equivalents (*SI Appendix,* Fig. S5 and Table S4). In addition, the model revealed other key residues such as L322 (*SI Appendix*, Fig. S6).

DN45 binding was restored on rat mGlu4 mutant bearing at least four human residues

The proposed model was further confirmed by introducing human-specific residues into the rat sequence, restoring DN45 binding and agonist activity on mutated rat mGlu4 receptor. We considered five human-specific residues based on their proximity to the apparent epitope of DN45 (i.e. I318, H323, D485, V385 and H507 (Fig. 3A)). When the five rat residues were mutated to their human equivalent (rmG4-5M), DN45 bound (Fig. 3D) and activated the receptor (Fig. 3E) with an affinity (K_D = 22.8 nM) and potency not different from those measured on human mGlu4 receptor (*SI Appendix*, Table S1, S2). The substitutions G485D (rmG4-1M), G485D+R323H (rmG4-2M) and G485D+R323H+S318I (rmG4-3M) on the rat mGlu4 receptor was however not sufficient to recover binding of DN45 (Fig. 3D). Indeed, the model of rmG4-3M reveals that DN45 is not able to interact with the three mutated residues (i.e. S318I, R323H, G485D) (Fig. S4A) because a loop is closing the entrance of the epitope cavity (*SI Appendix,* Fig. S7). The additional mutation of I385V or Q507H restores the opening of the cavity and allows for interactions between DN45 and the three key human residues (*SI Appendix,* Fig. S7). This was further supported when binding of DN45 to the rat mGlu4 bearing the three main aforementioned substitutions plus I385V (rmG4-4MB) or Q507H (rmG4-4MA) was recovered (Fig.

3D) and both mutants were activated by DN45 (Fig. 3E). The observed affinities (K_D = 13.6 nM and 10.4 nM, respectively) and potencies were not significantly different from those measured for human mGlu4 (Fig. 3D, E and *SI Appendix*, Table S1, S2). All mutants were functional as we successfully activated them with L-AP4 (*SI Appendix,* Fig. S3B).

Taken together, these modelling and mutagenesis data provide a reliable explanation for the species selectivity of DN45 by interacting with residues mainly located on lobe 2 of the VFT.

DN45 agonist activity needs interaction with both lobes of the VFT

The predictions of interactions between DN45 and lobe 1 of the VFT in a closed active state are especially comprising residues H371 to E401 (Fig. 4A, B and *SI Appendix*, Fig. S4B). Interactions with this region are expected to stabilize the closed conformation of the VFT, providing an explanation for the agonist activity of DN45 and its increased affinity for the active mGlu4 (Fig. 1D). In a first attempt to prevent the interaction between DN45 and lobe 1 of the mGlu4 VFT, an N-glycosylation site A399N/E401S was introduced. This resulted in a large decrease in DN45 agonist potency, but did not suppress its agonist activity (Fig. 4C).

Single-point mutations H371A, K386A, H392A, D397A, E401A and E403A did not lead to antagonist effects of DN45 on these mutants (*SI Appendix,* Fig. S8). Therefore, a virtual saturation mutagenesis was performed to predict the impact of multiple mutations of lobe 1 residues on the binding of DN45 but also the impact of these mutations on the overall stability of mGlu4. The best predicted mutations were H371E, R391M, R393W and A399K in a loop of lobe 1 (Fig. 4A, B). The calculated binding energy revealed that the highest destabilizing values were found for the triple

mutant R391M+R393W+A399K (4.82 kcal/mol) and quadruple mutant H371E+R391M+R393W+A399K (4.81 kcal/mol).

Experimental data support that this loop is involved in the agonist effect of DN45 as DN45 no longer activated neither the triple nor the quadruple mutant (Fig. 4D, E). Of note, the quadruple mutant displays constitutive activity that is reduced by DN45, revealing that DN45 acts as an inverse agonist on this receptor (Fig. 4E). This is confirmed by the significant antagonistic effect of DN45 on this mutant upon activation by L-AP4 (Fig. 4F and *SI Appendix*, Table S2).

Taken together, these data reveal that DN45 primarily binds to lobe 2, but also with lobe 1 in the active state, an interaction increasing its affinity, and required for its agonist activity.

DN45 acts as a positive allosteric modulator on heterodimeric mGlu2-4

It is now recognized that the mGlu4 subunit can associate with other mGlu subunits to form heterodimeric mGlu receptors (7, 8). Among these, the mGlu2-4 heterodimer has retained much attention and has specific pharmacological properties that were used to illustrate its existence in the brain (9, 10).

We first examined the binding of DN45 to the mGlu2-4 heterodimer using a combination of mGlu2 N-terminally labelled with CLIP-tag and C-terminal $GABA_{B1}$ endoplasmic reticulum retention sequence C1KKXX (21) (CLIP-mGlu2-C1KKXX) and mGlu4 N-terminally tagged with SNAP-tag and C-terminal $GABA_{B2}$ endoplasmic reticulum sequence C2KKXX (21) (SNAP-mGlu4-C2KKXX). After labelling CLIP-mGlu2-C1KKXX with Lumi4-Tb, binding of DN45 to the mGlu4 subunit should generate a TR-FRET signal between the Lumi4-Tb on the mGlu2 subunit and the d2 acceptor on an anti-c-Myc-antibody that binds to DN45 (Fig. 5A). A very low signal

could be detected under basal condition, that almost disappeared in the presence of the competitive antagonist LY341495 (Fig. 5B). However, a large signal could be measured in the presence of the mGlu4 agonist L-AP4, the general mGlu agonist glutamate, or the mGlu2 selective agonist LY379268 (Fig. 5B), revealing binding affinities of 5.0 nM, 3.1 nM and 7.4 nM, respectively, close to the K_D measured on the agonist occupied mGlu4 homodimers (3.1 nM).

The effect of DN45 on the conformation of the mGlu2-4 heterodimer was then examined. Using CLIP-mGlu2-C1KKXX labelled with O^6-benzylcytosine (BC)-Lumi4Tb and SNAP-mGlu4-C2KKXX labelled with BG-Green, only the heterodimer generates a TR-FRET signal that is largely decreased upon activation (10, 18). As previously reported, the mGlu2 agonist LY379268 activated the heterodimer, while the mGlu4 agonist L-AP4 remains very partial (10, 18). DN45 on the other hand could not activate the mGlu2-4 by itself (Fig. 5C). However, in the presence of a minimal concentration (EC_5) of LY379268 (50 nM), DN45 could activate the receptor, revealing a clear PAM effect (Fig. 5C). Indeed, DN45 largely increased the potency of the mGlu2 agonist LY379268 (Fig. 5D), demonstrating its potent pure PAM effect on the mGlu2-4 heterodimer.

Discussion

The mGlu4 receptor has been proposed as a potential drug target for the treatment of Parkinson’s disease (12, 22, 23) or pain (15). In the brain, mGlu4 can be found in a homodimeric form, or associated with other mGlu subunits, like mGlu2, in heteromeric complexes. Using ligands with different properties at mGlu4 homo- and heterodimers, evidence has been provided supporting homodimers as the best targets for Parkinson disease's treatment (13). However, the respective role of both

types of mGlu4 containing receptors remains to be clarified (8–10). In the present study we report an mGlu4 nanobody with selective agonist activity at mGlu4 homodimers, and with a pure PAM action on the mGlu2-4 heterodimers.

Nanobodies have become popular in pharmaceutical research. They have a high specificity and affinity and can stabilize specific conformations of their targets. Due to their small size compared to traditional IgG (~15 vs. ~150 kDa), nanobodies have several advantages like lower immunogenicity, better pharmacokinetics and the possibility to reach smaller cavities in proteins (3, 4). As such, nanobodies can stabilize specific conformations of their target, being interesting tools for structural studies (1) and innovative pharmacological agents (24). Moreover, some nanobodies can cross the blood-brain-barrier and can then be used to target the central nervous system (25). Of course, nanobodies may have a much better subtype selectivity than orthosteric ligands acting at a binding site often conserved in various receptor subtypes activated by the same natural ligand. Most recently described nanobodies with pharmacological action at GPCRs act as antagonists (26, 27) as is the first FDA-approved nanobody, caplacizumab (24).

Recently nanobodies acting as selective PAMs for mGlu2 (11) and mGlu5 (28) homodimers were reported, the formers having in vivo activities. Both nanobodies were found to stabilize the agonist bound active orientation of the two VFTs of the dimers, with the mGlu2 nanobodies acting at the active interface of the VFTs (11), while the mGlu5 one acts on a loop on the top of the mGlu5 VFT (28). Here we identified the mode of action of DN45 by combining state of the art modelling and docking approaches and mutagenesis. We show that DN45 can stabilize the closed active state of each VFT in the mGlu4 homodimer, as the binding epitope includes residues from both lobe 1 and lobe 2. DN45, like L-AP4, increases the same

proportion of mGlu4 in the active conformation, as shown by smFRET in the total absence of glutamate, demonstrating an agonist activity equivalent to that of L-AP4. While the primary binding epitope is located on lobe 2, further interaction between the VFT and DN45 occurs upon spontaneous closure of the VFT. These additional contacts increase the affinity of DN45 and lead to stabilization of the active state of the receptor, as does the agonist. This model is well supported by the observation that preventing the contact between lobe 1 and the nanobody through mutations, converts the nanobody into an antagonist or an inverse agonist, stabilizing the inactive receptor by preventing VFT closure. Taken together, our data confirm that stabilizing the closed VFTs is sufficient for receptor activation, even in the absence of glutamate. Such a mode of action is then different from what has been proposed for the mGlu2 and mGlu5 PAM nanobodies, and reveals novel ways for the development of selective agents acting at a specific mGlu subtype.

When tested on the mGlu2-4 heterodimer, DN45 was found unable to activate the receptor on its own. In contrast to the mGlu4 homodimer, on which two nanobodies are likely acting (one per VFT), only one is expected to bind to the heterodimer, on the mGlu4 VFT only. The fact that the nanobody cannot activate such a heterodimer suggests that the mGlu4 VFT may have less tendency to spontaneously close when associated with mGlu2. One may also consider the positive allosteric effect between each VFTs (21). The transient closure of one VFT may facilitate the closure of the other, such that binding of a first nanobody may facilitate the binding of the second one in the homodimer, leading to the stabilization of the active state without agonist, and then to the full agonist activity. Such an allosteric process is unlikely to occur in the heterodimer in the presence of DN45 alone, since DN45 only acts on one VFT. In agreement with this model, agonist binding in the mGlu2 VFT, largely favored DN45

binding on the mGlu4 subunit. Such a model is consistent with the pure PAM effect of DN45 observed on the mGlu2-4 heterodimer.

Such a PAM action of DN45 on mGlu2-4 is also consistent with the effects of group-III agonists acting at the mGlu4 VFT. Indeed, L-AP4 could barely activate the heterodimer, while it largely potentiates the effect of an mGlu2 agonist (10, 29). This supports the idea that the closure of the mGlu2 VFT is the driving force for the activation of the mGlu2-4 heterodimer, that is then further stabilized in the active state through the closure of the mGlu4 VFT by DN45.

This model points to a transactivation mechanism within the mGlu2-4 receptor, as the mGlu4 TMD is mainly responsible for G protein activation in this heterodimer (30). This is then similar to what is well established for the $GABA_B$ receptor in which GABA stabilizes the closed state of the GB1 VFT, leading to the G protein activation by the GB2 7TM (31).

Overall, we describe the first nanobody with a full agonist action at a GPCR. Such a tool will be useful to solve the active structure of human mGlu4. We show DN45 acts by stabilizing the closed state of the mGlu4 VFT, then through a novel mode of action compared to other nanobodies enhancing the activity of other class C GPCRs. Our study then provides a new insight in the activation mechanism of mGlu4 and mGlu2-4 receptors, and illustrates how powerful nanobodies can be to decipher the function of these different receptor subtypes.

Materials and Methods

Information on materials, llama immunization, selection, production and purification of DN45, mutagenesis, cell culture and transfection, labelling of CLIP and SNAP-tag, DN45 binding and selectivity assay, IP-1 accumulation assay, mGlu4 and mGlu2-4 biosensor assay, BRET assay, statistical analysis, single-molecule FRET approach and molecular modeling is provided in the *SI Appendix*.

Data availability

All data and associated protocols are available in the main paper and the *SI Appendix* and materials and methods upon request to J.-P.P.

Abbreviations

BC – O^6-benzylcytosine

BG – O^6-benzylguanine

BRET – Bioluminescence resonance energy transfer

CLIP-mGlu2-C1KKXX – mGlu2 N-terminally labelled with CLIP-tag and C-terminal endoplasmic reticulum retention sequence C1KKXX

DMEM – Dulbecco's Modified Eagle Medium

EAAC1 – Excitatory amino acid transporter 3

GABA - γ-amino butyric acid

GPCR – G protein-coupled receptor

IP1-d2 – Inositol phosphate labeled with d2

K_D – Equilibrium dissociation constant

mGlu – Metabotropic glutamate

NAM – Allosteric modulator limiting agonist-mediated responses

PAM – Allosteric modulator enhancing agonist-mediated responses

rmG4 – N-terminally SNAP-tagged rat mGlu4

rmG4-1M - N-terminally SNAP-tagged rat mGlu4 bearing one mutation (i.e. G485D)

rmG4-2M - N-terminally SNAP-tagged rat mGlu4 bearing two mutations (i.e. G485D, R323H)

rmG4-3M - N-terminally SNAP-tagged rat mGlu4 bearing three mutations (i.e. G485D, R323H, S318I)

rmG4-4MA - N-terminally SNAP-tagged rat mGlu4 bearing four mutations (i.e. S318I, R323H, G485D, I385V)

rmG4-4MB - N-terminally SNAP-tagged rat mGlu4 bearing four mutation (i.e. S318I, R323H, G485D, Q507H)

rmG4-5M – N-terminally SNAP-tagged rat mGlu4 bearing five mutations (i.e. S318I, R323H, G485D, I385V, Q507H)

RT-PCR – Reverse transcription polymerase chain reaction

smFRET – Single-molecule Förster resonance energy transfer

SNAP-mGlu4-C2KKXX - mGlu4 N-terminally tagged with SNAP-tag and a C-terminal endoplasmic reticulum sequence C2KKXX

TR-FRET – Time-resolved Förster resonance energy transfer

VFT – Venus flytrap domain

Acknowledgements and funding sources

We thank the ARPEGE platform facilities at the Institut de Génomique Fonctionnelle for all fluorescence-based assays. J.-P.P. was supported by la Fondation pour la Recherche Médicale (ref. DEQ20170336747), Cisbio Bioassays (EIDOS collaborative team IGF-CISBIO, ref. 039293) and LabEx MAbImprove (ref. NR-10-LABX-5301). P.R. was supported by the Agence Nationale de la Recherche (ref. ANR-15-CE18-0020-01). J.-P.P., L.P. and P.R. were further supported by the Centre National de la Recherche Scientifique and the Institut National de la Santé et de la Recherche Médicale. P.C. and D.N. were supported by the Fond Unique Interministériel of the French government (FUI, Cell2Lead project). F.A. was supported by the Centre National de la Recherche Scientifique and the Science Ambassador Program from Dassault Systèmes BIOVIA. J.H. was supported by a fellowship from la Région Occitanie and Cisbio Bioassays (TransACT, ref. 156544) and la Ligue contre le cancer (PhD grant, ref. IP/SC-16487). J.F. was supported by la Fondation pour la Recherche Médicale (ref. DEQ20170336747). R.Q. was supported by a grant from the Agence Nationale pour la Recherche (ANR 18-CE11-0004-02). The CBS belongs to the France-BioImaging national infrastructure supported by the French National Research Agency (ANR-10-INBS-04, “Investments for the future”).

References

1. K. D. Cromie, G. V. H. and C. Boutton, Nanobodies and their Use in GPCR Drug Discovery. *Curr. Top. Med. Chem.* **15**, 2543–2557 (2015).
2. A. Gupta, *et al.*, Increased Abundance of Opioid Receptor Heteromers Following Chronic Morphine Administration. *Sci. Signal.* **3** (2010).
3. C. J. Hutchings, M. Koglin, W. C. Olson, F. H. Marshall, Opportunities for therapeutic antibodies directed at G-protein- coupled receptors. *Nat. Rev. Drug Discov.* **16**, 787–810 (2017).
4. T. Hino, T. Arakawa, H. Iwanari, T. Yurugi-kobayashi, G protein-coupled receptor inactivation by an allosteric inverse-agonist antibody. *Nature* **482**, 237–240 (2012).
5. A. S. Hauser, M. M. Attwood, M. Rask-Andersen, H. B. Schiöth, D. E. Gloriam, Trends in GPCR drug discovery: New agents, targets and indications. *Nat. Rev. Drug Discov.* **16**, 829–842 (2017).
6. J. Kniazeff, L. Prézeau, P. Rondard, J. Pin, C. Goudet, Dimers and beyond : The functional puzzles of class C GPCRs. *Pharmacol. Ther.* **130**, 9–25 (2011).
7. E. Doumazane, *et al.*, A new approach to analyze cell surface protein complexes reveals specific heterodimeric metabotropic glutamate receptors. *FASEB J.* **25**, 66–77 (2011).
8. J. Lee, *et al.*, Defining the Homo- and Heterodimerization Propensities of Metabotropic Glutamate Receptors. *Cell Rep.* **31**, 107605 (2020).
9. S. Yin, *et al.*, Selective actions of novel allosteric modulators reveal functional heteromers of Metabotropic glutamate receptors in the CNS. *J. Neurosci.* **34**, 79–94 (2014).
10. D. M. Delgado, *et al.*, Pharmacological evidence for a metabotropic glutamate receptor heterodimer in neuronal cells. *Elife* **6**, 1–33 (2017).
11. P. Scholler, *et al.*, Allosteric nanobodies uncover a role of hippocampal mGlu2 receptor homodimers in contextual fear consolidation. *Nat. Commun.* **8**, 1 (2017).
12. D. Charvin, mGlu4 allosteric modulation for treating Parkinson's disease. *Neuropharmacology* **135**, 308–315 (2018).
13. C. M. Niswender, *et al.*, Development and Antiparkinsonian Activity of VU0418506, a Selective Positive Allosteric Modulator of Metabotropic Glutamate Receptor 4 Homomers without Activity at mGlu2/4 Heteromers. *ACS Chem. Neurosci.* **7**, 1201–1211 (2016).
14. P. Gubellini, C. Melon, E. Dale, D. Doller, L. Kerkerian-Le Goff, Distinct effects of mGlu4 receptor positive allosteric modulators at corticostriatal vs. striatopallidal synapses may differentially contribute to their antiparkinsonian action. *Neuropharmacology* **85**, 166–177 (2014).
15. B. Vilar, *et al.*, Alleviating pain hypersensitivity through activation of type 4 metabotropic glutamate receptor. *J. Neurosci.* **33**, 18951–18965 (2013).
16. C. Zussy, *et al.*, Dynamic modulation of inflammatory pain-related affective and sensory symptoms by optical control of amygdala metabotropic glutamate receptor 4. *Mol. Psychiatry* **23**, 509–520 (2018).
17. K. Even-Desrumeaux, *et al.*, Masked selection: A straightforward and flexible approach for the selection of binders against specific epitopes and differentially expressed proteins by phage display. *Mol. Cell. Proteomics* **13**, 653–665 (2014).
18. P. Scholler, *et al.*, HTS-compatible FRET-based conformational sensors clarify

membrane receptor activation. *Nat. Chem. Biol.* **13**, 372–380 (2017).
19. R. Chen, L. Li, Z. Weng, ZDOCK : An Initial-Stage Protein-Docking Algorithm. *PROTEIN Struct. Funct. Genet.* **52**, 80–87 (2003).
20. B. Pierce, Z. Weng, ZRANK: Reranking Protein Docking Predictions With an Optimized Energy Function. *PROTEIN Struct. Funct. Genet.* **67**, 1078–1086 (2007).
21. J. Kniazeff, *et al.*, Closed state of both binding domains of homodimeric mGlu receptors is required for full activity. *Nat. Struct. Mol. Biol.* **11**, 706–713 (2004).
22. S. Urwyler, Allosteric modulation of family C G-protein-coupled receptors: from molecular insights to therapeutic perspectives. *Pharmacol. Rev.* **63**, 59–126 (2011).
23. I. Sebastianutto, M. A. Cenci, mGlu receptors in the treatment of Parkinson ' s disease and L-DOPA-induced dyskinesia. *Curr. Opin. Pharmacol.* **38**, 81–89 (2018).
24. S. Duggan, Caplacizumab : First Global Approval. *Drugs* **78**, 1639–1642 (2018).
25. T. Li, *et al.*, Cell-penetrating anti-GFAP VHH and corresponding fluorescent fusion protein VHH-GFP spontaneously cross the blood-brain barrier and specifically recognize astrocytes: Application to brain imaging. *FASEB J.* **26**, 3969–3979 (2012).
26. S. Low, *et al.*, VHH antibody targeting the chemokine receptor CX3CR1 inhibits progression of atherosclerosis. *MAbs* **12**, 1–12 (2020).
27. C. McMahon, *et al.*, Synthetic nanobodies as angiotensin receptor blockers. *Proc. Natl. Acad. Sci. U. S. A.* **117**, 20284–20291 (2020).
28. A. Koehl, *et al.*, Structural insights into the activation of metabotropic glutamate receptors. *Nature* **566**, 79–84 (2019).
29. J. Levitz, *et al.*, Mechanism of Assembly and Cooperativity of Homomeric and Heteromeric Metabotropic Glutamate Receptors. *Neuron* **92**, 143–159 (2016).
30. J. Liu, *et al.*, Allosteric control of an asymmetric transduction in a G protein-coupled receptor heterodimer. *Elife* **6**, 1–19 (2017).
31. T. Galvez, *et al.*, Allosteric interactions between GB1 and GB2 subunits are required for optimal $GABA_B$ receptor function. *EMBO J.* **20**, 2152–2159 (2001).
32. I. Brabet, M. Parmentier, C. De Colle, Comparative effect of L -CCG-I , DCG-IV and k -carboxy- L -glutamate on all cloned metabotropic glutamate receptor subtypes. *Neuropharmacology* **37**, 1043–1051 (1998).
33. P. Scholler, *et al.*, HTS-compatible FRET-based conformational sensors clarify membrane receptor activation. *Nat. Chem. Biol.* **13**, 372–380 (2017).
34. A. Cao, R. B. Quast, F. Fatemi, P. Rondard, Allosteric modulators enhance agonist efficacy by increasing the residence time of a GPCR in the active state. *bioRxiv*, 1–37 (2021).
35. L. Olofsson, *et al.*, Fine tuning of sub-millisecond conformational dynamics controls metabotropic glutamate receptors agonist efficacy. *Nat. Commun.* **5** (2014).
36. A. Sali, T. L. Blundell, Comparative Protein Modelling by Satisfaction of Spatial Restraints. *J. Mol. Biol.* **234**, 779–815 (1993).
37. M. Shen, A. Sali, Statistical potential for assessment and prediction of protein structures. *Protein Sci.* **15**, 2507–2524 (2006).
38. J. C. Phillips, *et al.*, Scalable Molecular Dynamics with NAMD. *J. Comput. Chem.* **26**, 1781–1802 (2005).
39. V. Z. Spassov, L. Yan, pH-Selective mutagenesis of protein–protein interfaces:

In silico design of therapeutic antibodies with prolonged half-life. *PROTEINS Struct. Funct. Bioinforma.* **81**, 704–714 (2012).
40. V. Z. Spassov, L. Yan, A pH-dependent computational approach to the effect of mutations on protein stability. *J. Comput. Chem.* **37**, 2573–2587 (2016).
41. V. Z. Spassov, L. Yan, P. K. Flook, The dominant role of side-chain backbone interactions in structural realization of amino acid code. ChiRotor: A side-chain prediction algorithm based on side-chain backbone interactions. *Protein Sci.* **16**, 494–506 (2007).

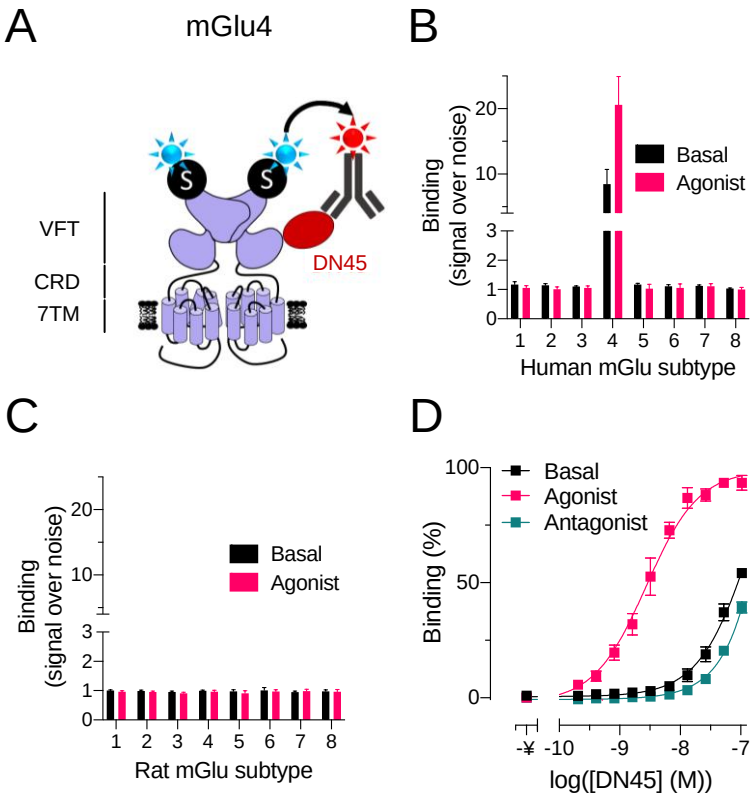

Fig. 1. DN45 is selective for the human mGlu4 receptor and preferentially binds to the active receptor. *(A)* Cartoon representing a TR-FRET-based binding assay. SNAP-mGlu receptors were labelled with 100 nM BG-Lumi4-Tb (blue star). Then, 100 nM of DN45 containing a c-Myc epitope was labelled with 200 nM of an anti-c-Myc-antibody (gray) coupled to d2 (red star). *(B)* Specific binding of DN45 to human mGlu4 receptor without (black) and with (pink) saturating concentration of agonist (mGlu group-I: 1 µM quisqualic acid, group-II: 100 nM LY379268, group-III: 10 µM L-AP4), represented by an increase of signal compared to an irrelevant nanobody containing the c-Myc sequence. *(C)* No specific binding was observed between the nanobody and any rat mGlu receptors in absence (black) or presence (pink) of agonist. *(D)* Binding of increasing concentration of DN45 on hmGlu4 under basal condition (black), in presence of the agonist L-AP4 (10 µM), or in the presence of the

antagonist LY341495 (100 μM). Data in *B-D* are mean ± SEM of three individual experiments (*SI Appendix,* Table S1).

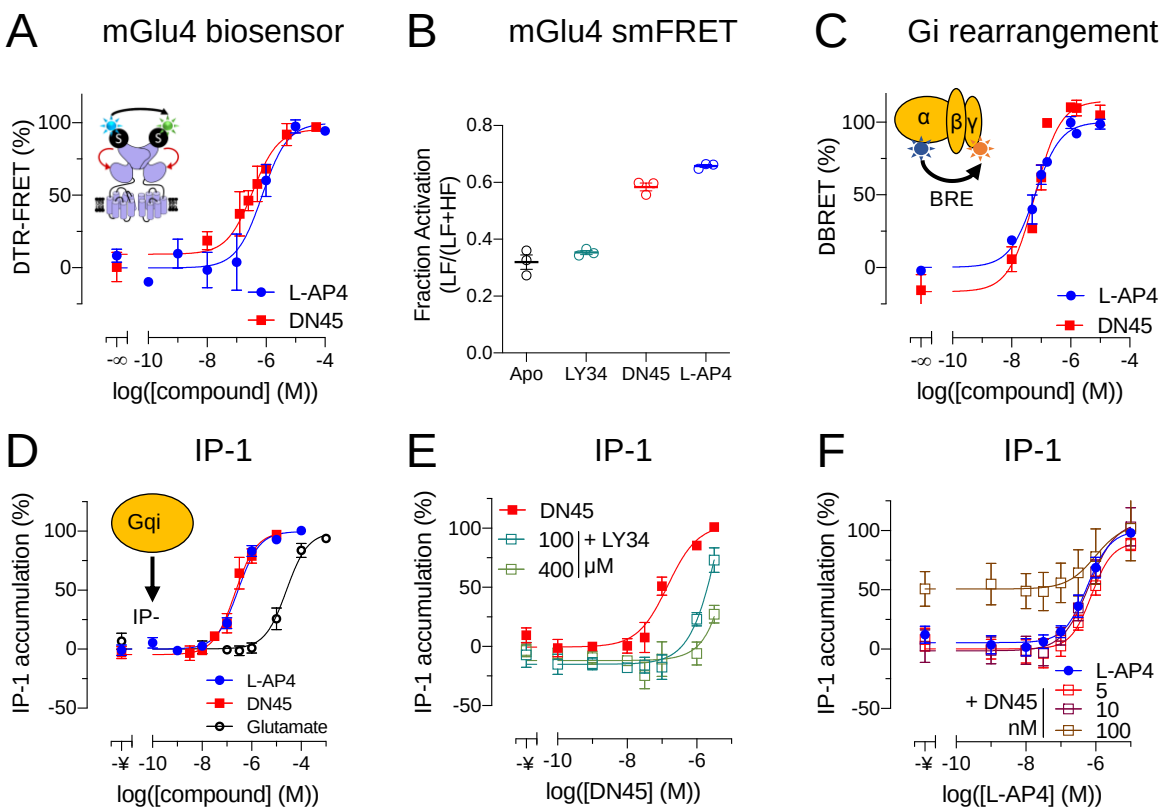

Fig. 2. DN45 is a full agonist of the hmGlu4 receptor. *(A)* Measurement of the change in TR-FRET induced upon stimulation with increasing concentrations of L-AP4 (blue) or DN45 (red). (B) Measurement of the fraction of activated receptor by single molecule FRET in basal/apo state (black), in presence of LY341495 (green), DN45 (red) or L-AP4 (blue). *(C)* Measurement of the rearrangement of the Gi protein in a BRET experiment upon stimulation with increasing concentrations of L-AP4 (blue) and DN45 (red). *(D)* Measurements of the activation of the Gq pathway via transient overexpression of Gqi9 upon stimulation with increasing concentrations of L-AP4 (blue), DN45 (red) or glutamate (black). *(E)* Measurements of the activation of the Gq pathway via transient overexpression of Gqi9 upon stimulation with increasing concentrations of DN45 alone (red) or in presence of LY341495 (i.e. 100 or 400 µM) *(F)* Measurement of the activation of the Gq pathway upon stimulation with increasing concentrations of L-AP4 alone (blue) or L-AP4 with non-saturating concentrations (i.e. 5, 10 or 100 nM) of DN45. Data of *A-F* are mean ± SEM of three

or more individual experiments. Statistical analysis for *A-D* was performed using unpaired two-tailed t test and statistical analysis of *F* was ordinary one-way ANOVA with Dunnett's multiple comparisons test (*SI Appendix,* Table S2 and S3).

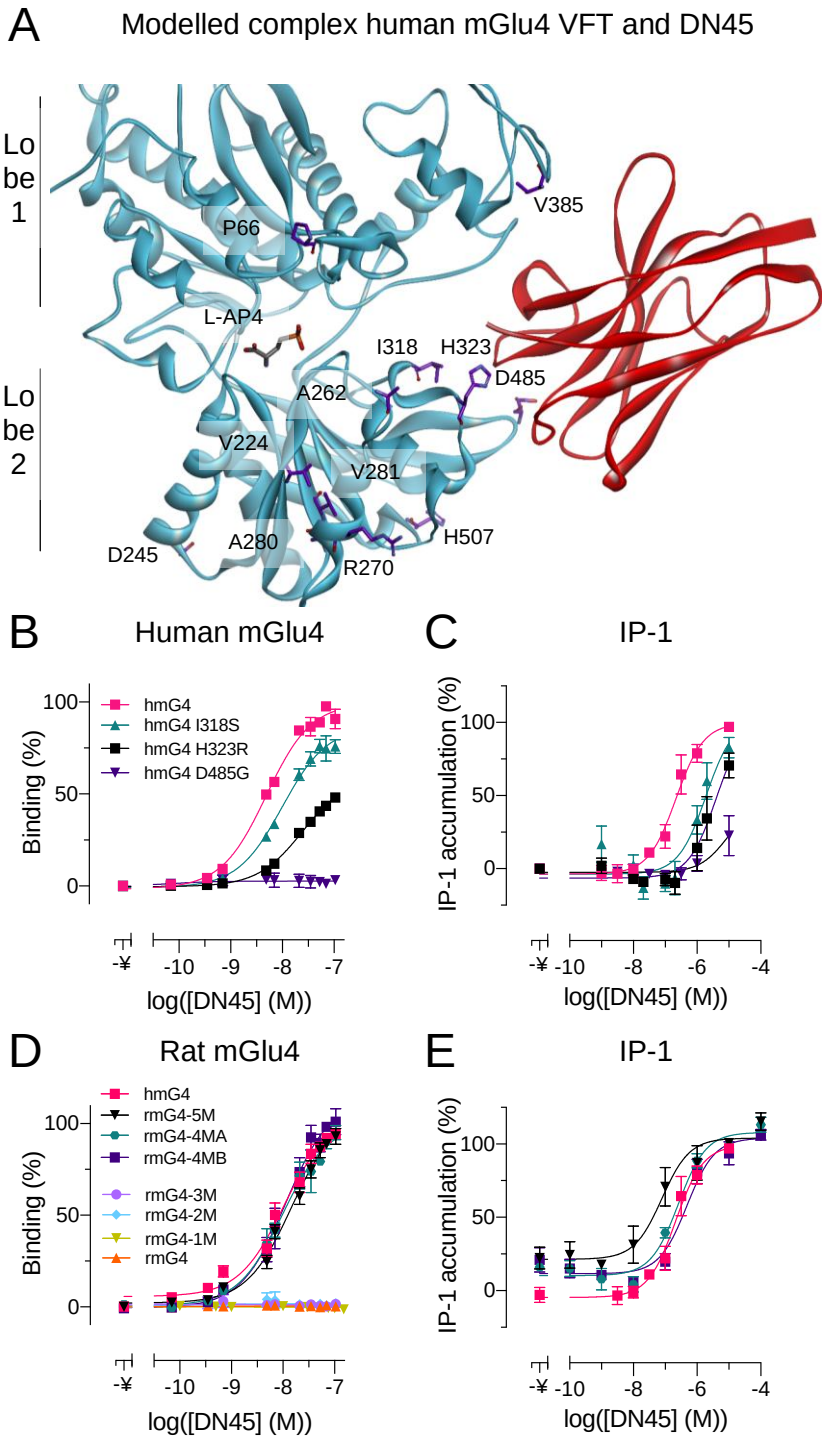

Fig. 3. Residues in lobe 2 of the human mGlu4 VFT confer subtype selectivity to DN45. *(A)* Front view of the closed conformation of the VFT of the human mGlu4 receptor, stabilized by DN45 (red) in the best-scored non-constrained docking

followed by 10 ns molecular dynamics simulation. Residues on the surface of the mGlu4 VFT that are specific for the human orthologue are highlighted in purple (side chains). *(B)* Binding of DN45 was determined in the TR-FRET binding assay as illustrated in Fig. 1A. with human WT (hmG4) and mutated-mGlu4 receptors (i.e. hmG4 I318S, hmG4 H323R or hmG4 D485G) in the presence of 1 µM L-AP4. *(C)* Activation of the Gq pathway by hmG4, hmG4 I318S, hmG4 H323R and hmG4 D485G with increasing concentrations of DN45. *(D)* Binding of DN45 to mutated rat mGlu4 receptors rmG4-5M (K_D = 22.8 nM), rmG4-4MA (K_D = 10.4 nM), rmG4-4MB (K_D = 13.6 nM) is not significantly different than to hmG4 (K_D = 5.4 nM) and no binding is observed for rmG4-3M, rmG4-2M, rmG4-M1 and rmG4. *(E)* DN45 activation of the Gq pathway by rmG4-5M, rmG4-4MA and rmG4-4MB. Data of *B-E* are mean ± SEM of three or more individual experiments. The K_D values and statistical analysis for *B-E* was performed using ordinary one-way ANOVA with Dunnett's multiple comparisons test and are presented in *SI Appendix (*Table S1, S2).

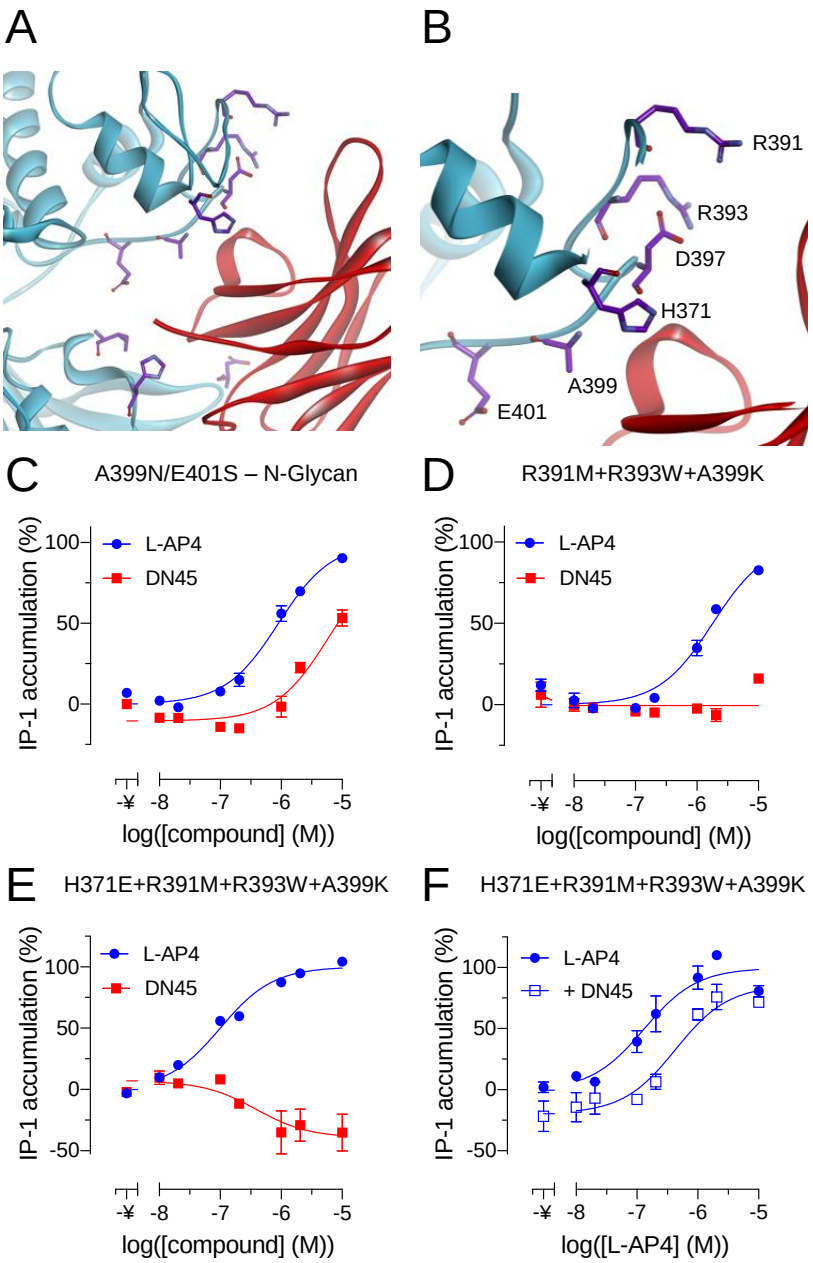

Fig. 4. DN45 agonist activity needs interactions with lobe 1 of the VFT. *(A)* A front view of the interactions between DN45 and lobe 1 and lobe 2 of the human mGlu4 receptor. Residues on lobe 1 in the loop spanning from H371 to E401 and residues I318, H323 and D485 are highlighted in purple (side chains). *(B)* A zoom on the loop comprising residues H371 to E401. *(C)* IP-1 production by L-AP4 (blue) and DN45 (red) of a human mGlu4 receptor bearing a N-glycosylation site at N399. *(D)* Effect of L-AP4 (blue) and DN45 (red) on IP-1 production by a human mGlu4

receptor bearing three mutations (i.e. R391M, R393W and A399K). *(E)* Effect of L-AP4 (blue) and DN45 (red) on a human mGlu4 receptor bearing four mutations (i.e. H371E, R391M, R393W and A399K). *(F)* Effect of L-AP4 alone (filled circles) and in the presence of 100 nM DN45 (open squares) on the activity of the quadruple hmGlu4 receptor mutant. Data of *C-F* are mean ± SEM of three individual experiments. Statistical analysis of *C* and F is performed using unpaired one-tailed t test (*SI Appendix,* Table S2).

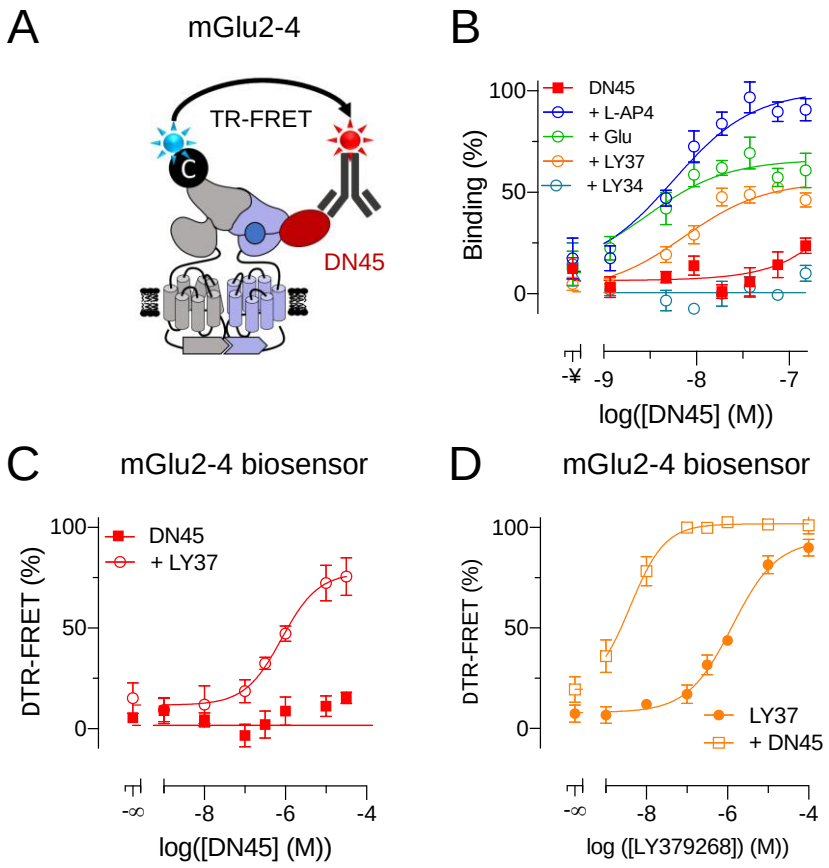

Fig. 5. DN45 acts as a positive allosteric modulator on heterodimeric mGlu2-4 *(A)* A cartoon representing a TR-FRET-based assay to measure binding of DN45 to the mGlu2-4 heterodimer using CLIP-mGlu2-C1KKXX and SNAP-mGlu4-C2KKXX. *(B)* Binding of DN45 to mGlu2-4 alone (red), in the presence of 100 µM mGlu4 antagonist LY341495 (light blue), of 1 mM glutamate (green), of 10 µM LY379268 (orange), or of 10 µM L-AP4 (blue). *(C)* Activation of the mGlu2-4 heterodimer by DN45 alone (red) or in the presence of the mGlu2 agonist LY379268 (50 nM) measured by a TR-FRET biosensor using CLIP-mGlu2-C1KKXX and SNAP-mGlu4-C2KKXX, labelled with 1 µM BC-Green and 100 nM BG-Lumi4Tb. *(D)* The response of LY379268 (filled circles) on the TR-FRET biosensor is potentiated by 10 µM DN45 (open squares). Data of *B-D* are mean ± SEM of three or more individual experiments. Statistical analysis of *B* is performed using ordinary one-way ANOVA with Tukey's multiple comparisons test and analysis of *D* is performed using ordinary

one-way ANOVA with Dunnett's multiple comparisons test (*SI Appendix,* Table S1, S2).

Supplementary Information Text

Materials

L-AP4 (Cat. No. 0103), LY341495 (Cat. No. 1209/1), LY379268 (Cat. No. 2453) and L-Quisqualic acid (Cat. No. 0.188) were bought from Tocris Bioscience. Isopropyl β-D-1-thiogalactopyranoside (IPTG) (ref. I6758), L-glutamic acid hydrochloride (ref. G2128) and Poly-L-Ornithine (ref. P4957) were from Sigma-Aldrich. O^6-benzylcytosine (BC)-Lumi4-Tb (ref. SCLPTBF), BC-Green (ref. SCLPGRNF), O^6-benzylguanine (BG)-Lumi4Tb (ref. SSNPTBX), BG-Green (ref. SSNPGRNZ), anti-c-Myc-d2 (ref. 61MYCDAF) and Tag-lite® buffer (ref. LABMED) were kindly supplied by Cisbio Bioassays. BG-Cy3b was custom designed by Cisbio. The plasmids encoding for the N-terminal SNAP-tag and CLIP-tag-labelled wild-type human and rat mGlu4 (18), rat mGlu2-C1KKXX (7) and rat SNAP-mGlu4-C2KKXX (30) have been described previously.

Methods

Llama immunization, selection, production and purification of DN45

The llama immunization, selection, production and purification of DN45 were performed as described previously (11). In brief, two llamas were immunized by four subcutaneous injections with 5×10^7 HEK293T cells, transfected with rat or human mGlu4 receptors. The V_HH library constructions were performed in *E. Coli* TG1 strains and the library diversity was above 10^9 transformants.

Bacteria were then infected by KM13 helper phage and phage-containing pellets were purified by two selection rounds on human mGlu4 receptor transfected in HEK293T (2×10^7) cells. Each round was preceded by a depletion step on cells that were not transfected and positive selections were performed in the presence of an excess of anti-HEK293 cells (17). *E. Coli* TG1 bacteria were infected with eluted phages and could be used for production of the nanobody.

The production of DN45 was done by transforming *E. Coli* BL21DE3 strain bacteria. They were grown overnight at 37 °C while agitating. Protein production was induced the day after by addition of 1 mM IPTG and bacteria were grown overnight at 28 °C while agitating. Bacteria were then collected and lysed in TES-buffer containing Tris, EDTA and sucrose. After centrifugation, the periplasmic extract was recovered and the His-tagged nanobodies were purified by Ni-NTA purification (Qiagen).

Mutagenesis

For the generation of rmG4-2M, rmG4-3M, rmG4-4MA, rmG4-4MB and rmG4-5M, synthethic genes encoding for the rat mGlu4 with corresponding mutations were ordered at GeneCust. The synthetic gene was inserted in a N-terminally SNAP-tagged rat mGlu4 receptor with the DNA ligation kit from Agilent Technologies.

SNAP-rmG4-5M-C2KKXX was generated by introducing the synthetic gene encoding for rmG4-5M into a N-terminally SNAP-tagged rat mGlu4 receptor with a C-terminal endoplasmic reticulum sequence C2KKXX. All other mutations were done by site-directed mutagenesis following the QuickChange mutagenesis protocol from Agilent Technologies.

Cell culture and transfection

HEK-293 (ATCC® CRL-1573™) cells were cultured in Dulbecco's Modified Eagle Medium (DMEM) (ref. 41965, Gibco™) containing 10% fetal bovine serum (FBS) (ref. F2442, Sigma-Aldrich). For each experiment we used 100,000 cells/well of a black 96-wells plate (ref. 655086, Greiner bio-one) coated with poly-L-ornithine (ref. P4957, Sigma-Aldrich). Cells were detached from the petridish (~80% confluency) with trypsin-EDTA (0.05%) (ref. 25300054, Gibco™) and after removal of the trypsin-EDTA by centrifuging, diluted in DMEM supplemented with 10% FBS.

Depending on the experiment, HEK-293 cells were transfected by electroporation (32) or reverse lipofectamine transfection following the manufacturer's protocol (Invitrogen™ Lipofectamine 2000™). To prevent toxic concentrations of glutamate in the medium, excitatory amino acid transporter 3 (EAAC1) was co-transfected. For binding experiments 9 µg of plasmid of the receptor and 1 µg EAAC1 were co-transfected by electroporation. For IP-1 accumulation experiments, 8 µg of plasmid of the receptor, 1 µg Gqi9 and 1 µg EAAC1 were co-transfected by electroporation. For the Gi-BRET assay, 4 µg of plasmid of the receptor, 0.8 µg Gi-Rluc, 0.8 µg Gβ, 1.6 µg Gγ-Venus and 1 µg EAAC1 were co-transfected by electroporation. For the mGlu2-4 biosensor experiment, 80 ng CLIP-mGlu2-C1KKXX, 40 ng SNAP-rmG4-5M-C2KKXX, 20 ng EAAC1 and 10 ng pRK6 empty vector per well were transfected by

reverse lipofectamine transfection. Cells were incubated for 24 hours at 37 °C and 5% CO_2 and medium was changed for pre-heated serum-free DMEM Glutamax (ref. 10566016, Gibco™) 2 hours before the start of the experiment.

Labelling of CLIP and SNAP-tag

Labelling of the CLIP and SNAP-tag with fluorescent molecules was done for 1 hour and 30 minutes at 37 °C in serum-free DMEM Glutamax. For expression and binding experiments for the mGlu4, the cells were incubated with 100 nM BG-Lumi4Tb. For measuring expression levels of the mGlu2-4, the cells were incubated with 1 µM BC-Lumi4Tb and 100 nM BG-Lumi4Tb. For binding on the mGlu2-4, the cells were incubated with 1 µM BC-Lumi4Tb. For the TR-FRET biosensor assay of the mGlu4, the cells were incubated with 100 nM BG-Lumi4Tb and 60 nM BG-Green. For the TR-FRET biosensor assay of the mGlu2-4, the cells were incubated with 100 nM BG-Lumi4Tb and 1 µM BC-Green. Unbound substrate was removed by washing each well four times with Tag-lite®-buffer.

DN45 binding and selectivity assay

Eight rat and eight human mGlu receptors were overexpressed in HEK293 cells as described in cell culture and transfection and incubated in a black 96-wells plate. Expression levels of the receptors were measured by the PHERAstar FS as the signal at 620 nm after excitation at 337 nm by a UV-pulsed nitrogen laser. Next, cells were pre-incubated for 30 minutes at 37 °C and 5% CO_2 with 10 µM L-AP4, 100 nM LY379268, 1 µM quisqualic acid or 100 µM LY341495 in Tag-lite®-buffer depending on the overexpressed receptor. Then,105 nM of DN45 and 200 nM anti-c-Myc-d2 were added at the same time and cells were incubated for 3 hours at 20 °C. As a

negative control, a nanobody against β-arrestin 2 containing the c-Myc sequence was added instead of DN45. TR-FRET was measured with the PHERAstar FS after excitation at 337 nm by a UV-pulsed nitrogen laser. Signals at 620 nm and 665 nm were integrated and the HTRF®-ratio was calculated as follows:

$$HTRF® - ratio = \frac{Signal\ 665\ nm}{Signal\ 620\ nm} \times\ 10{,}000$$

Values were normalized as the signal over the signal of the negative control.

IP-1 accumulation assay

Inositol phosphate (IP-1) accumulation was determined with the IP-One assay kit from Cisbio Bioassays (ref. 62IPAPEC). Cells had been prepared in a black 96-wells plate. Dilution ranges of DN45 and L-AP4 were prepared in stimulation buffer, added to the cells and incubated for 30 minutes at 37 °C and 5% CO_2. Then, cells were lysed by addition of IP1 labelled with d2 and anti-IP1 antibody labelled with Lumi4Tb in lysis buffer. The lysate was incubated for 1 hour at 20 °C and TR-FRET was measured with the PHERAstar FS and the HTRF®-ratio was determined. Values were normalized as the percentage of response to L-AP4.

mGlu2-4 and mGlu4 biosensor assay

Compounds were added to each well of a black 96-wells plate containing cells and incubated for 30 minutes at 37 °C and 5% CO_2 in Tag-lite®-buffer. In case of pre-incubation steps, compounds were pre-incubated 30 minutes at 37 °C and 5% CO_2 prior to addition of the other compounds. TR-FRET was measured with the PHERAstar FS after excitation at 337 nm by a UV-pulsed nitrogen laser. The signal at 520 nm was integrated and an acceptor ratio was calculated as described before (33):

$$Acceptor\ ratio\ (\mu s) = \frac{\int_{100}^{50} Signal\ at\ 520\ nm}{\int_{1600}^{1200} Signal\ at\ 520\ nm}$$

Values were normalized as the percentage of response to L-AP4.

BRET assay

Cells had been prepared in a black 96-wells plate. Coelenterazine and dilution ranges of DN45, L-AP4 were prepared in PBS buffer. The signals at 530 nm and 480 nm were measured by the Mithras LB 940 (Berthold). Coelenterazine was added and signals were measured for 10 minutes. Then, coelenterazine and compounds were added directly after each other. Signals were measured for 25 minutes and BRET-values were calculated by dividing the signals at 530 nm and 480 nm. Values were normalized as percentage of response to L-AP4.

Statistical analysis

Curve fitting and statistical analysis was done with Graphpad Prism software (version 9.0). Data are expressed as mean ± SEM of three or more individually performed experiments. The performed statistical analysis is explained in the corresponding figure legend. P-values<0.05 were considered significant.

Single-molecule FRET approach

Sample preparation and smFRET measurements

Sample preparation and smFRET measurements were done as previously described(34) with a few modifications as specified in the following.

Cell culture, transfection and membrane fraction preparation

HEK293T cells (ATCC CRL-3216, LGC Standards S.a.r.l., France) were grown in Gibco™ DMEM, high glucose, GlutaMAX™ Supplement, pyruvate (Thermo Fisher Scientific, France) supplemented with 10% (vol/vol) FBS (Sigma-Aldrich, France) at 37°C, 5% CO_2 in 25cm^2 flasks to approximately 80 % confluence. Transfection was carried out by mixing 4 µg SNAP-mGlu4 plasmid DNA and 8 µl Lipofectamine 2000 (Thermo Fisher Scientific, France) in 500 µl Gibco™ Opti-MEM™ I reduced serum medium (Thermo Fisher Scientific, France) and incubation at room temperature for 25 minutes. The mixture was then added to the cells in DMEM GlutaMax supplemented with10 % FBS and expression was carried out for 72h at 37°C and 5% CO_2. The medium was replaced once with fresh DMEM GlutaMax with 10 % FBS after 48h. SNAP-tag labeling was achieved by addition of 2 mL DMEM GlutaMax supplemented with 900 nM BG-Cy3b and 300 nM BG-d2 and carried out for 1.5 hours at 37°C and 5 % CO_2, followed by three washes with 5 mL PBS DPBS w/o Ca^{2+} and Mg^{2+} (Thermo Fischer Scientific, France) at ambient temperature. Then cells were detached mechanically using a cell scraper in DPBS and collected at 1000 x g and 22°C for 5 minutes. Cells were resuspended in cold hypotonic lysis buffer (10 mM HEPES pH 7.4, cOmplete™ protease inhibitor (Sigma-Aldrich, France)), frozen and stored at -80°C. For the preparation of membrane fractions cells were thawed on ice and passed 30-times through a 200 µL pipette tip. After two rounds of centrifugation at 500 x g and 4°C for 5 min, the supernatant was aliquoted and centrifuged at 21,000 x g and 4°C for 30 min to collect crude membranes. The pellets were washed once with 20 mM HEPES pH 7.4, 118 mM NaCl, flash frozen in liquid N_2 and stored at -80°C.

Detergent solubilization

Receptors were solubilized on ice by resuspension of crude membranes in acquisition buffer (20 mM Tris-HCl pH7.4, 118 mM NaCl, 1.2 mM KH_2PO_4, 1.2 mM $MgSO_4$, 4.7 mM KCl, 1.8 mM $CaCl_2$) supplemented with 1 % (w/v) lauryl maltose neopentyl glycol (LMNG, Anatrace purchased through CliniSciences, France) + 0.2 % (w/v) cholesteryl hemisuccinate tris salt (CHS Tris, Anatrace purchased through CliniSciences, France) for 5 min. Then Glyco-diosgenin (GDN, Avanti Polar Lipids purchased through Merck) was added (final detergent concentration 0.83 % LMNG + 0.167 % CHS Tris + 0.83 % GDN) and the solution was centrifuged for 10 min at 21,000 x g and 4°C. The supernatant was diluted 8.33-times in acquisition buffer and applied to a Zeba Spin Desalting Column (7 kDa cut-off, Thermo Fisher Scientific, France) equilibrated in acquisition buffer containing 0.005 % LMNG + 0.001 % CHS Tris + 0.005 % GDN and centrifuged 2 min at 1,500 x g and 4°C. The flow-through was then immediately diluted 10-times in cold acquisition buffer and kept on ice in the dark until use.

smFRET measurements

The pulsed interleaved excitation (PIE) – multiparameter fluorescence detection (MFD) setup, data acquisition and analysis were previously described.(34) Measurements were performed at a 4 times dilution of the sample in acquisition buffer without detergent and further dilution in acquisition buffer containing 0.0025 % LMNG, 0.0005 CHS tris, 0.0025 % GDN to achieve single molecule-compatible concentrations of labeled receptors (approximately 30-50 pM) in the absence of ligand or in presence of 100 µM LY34, 10 µM DN45 or 10 µM L-AP4. Apparent FRET efficiencies (E_{PR}) corrected for direct acceptor excitation and donor leakage into the acceptor channel were determined using the Software Package for Multiparameter Fluorescence Spectroscopy, Full Correlation and Multiparameter Fluorescence

Imaging developed in C.A.M. Seidel's lab (http:// www.mpc.uni-duesseldorf.de/seidel/) as previously described.(35) FRET histograms were fitted using Origin 6 (Microcal Software, Inc.) and displayed in GraphPad Prism 7.05.

Molecular modelling

Homology model of mGlu4 VFT

The model for the mGlu4 homodimer was built using MODELER (36) as implemented in Discovery Studio. Two PDB structures 6BSZ (Human mGlu8 Receptor complexed with glutamate at 2.65 Å resolution) and 6BT5 (Human mGlu8 Receptor complexed with L-AP4 at 2.92 Å resolution) were used as templates. A disulfide bridge was defined between the Cys 136 of the two loops. The ligand L-AP4 from 6BT5 was used when constructing the model. We generated 100 models and the one with the lowest probability density factor (PDF) and lowest discrete optimized protein energy (DOPE) (37) score was selected.

Homology model of DN45

We then built the homology model of DN45 with the Model Antibody Cascade protocol from Discovery Studio 2020. This protocol automatically identified most similar PDB structures to model the framework and used 5GXB, 5IMM, 4LGS and 5M2W. The protocol also identifies the best templates for each CDR loop. For loop H1, it used loop H1 from PDB structures 5LMJ and EJ1. For loop H2, the templates were the H2 loop from 6EHG, 4TVS. Finally, for loop H3, the templates loops where from 5LWF and 1U0Q.

Docking of DN45 to mGlu4 VFT

The docking of DN45 to mGlu4 VFT was performed with ZDOCK (19) as implemented in Discovery Studio (BIOVIA, Dassault Systèmes, Discovery Studio Modeling Environment, Release 2020, San Diego: Dassault Systèmes, 2020). After generating 54000 poses, a filtering was then used to keep only poses where CDRs from the nanobody DN45 were interacting with mGlu4. The distance criterion was 10 Å. The two first poses with the best ZRANK (20) score were in the same cluster, at the interface of the two lobes.

Refinement of Docked Structures

In order to refine the best pose generated with ZDOCK, we solvated the mGlu4 dimer-DN45 complex and the mGlu4 dimer-DN45-L-AP-4 complex in an orthorhombic periodic box of water with a minimum distance from boundary of 15.0 Å and performed with NAMD (38) a molecular dynamics simulation for 10 ns for each system. Analysis of trajectories and non-bonded interactions have been performed with Discovery Studio.

Virtual mutations

Using the last frame of the molecular dynamics simulation, we performed a virtual mutagenesis to identify residues in mGlu4 that are critical for binding to DN45. We used the Discovery Studio Calculate Mutation Energy Binding protocol (39) that evaluates the effect of mutations on the binding affinity of molecular partners in protein-protein and protein-ligand complexes. It performs combinatorial amino-acid scanning mutagenesis on a set of selected amino-acid residues by mutating them to one or more specified amino-acid types. The energy effect of each mutation on the binding affinity ($\Delta\Delta G_{mut}$) is calculated as the difference between the binding free

energy ($\Delta\Delta G_{bind}$) in the mutated structure and wild type protein: $\Delta\Delta G_{mut}$ = $\Delta\Delta G_{bind}$(mutant) - $\Delta\Delta G_{bind}$(wild type). The $\Delta\Delta G_{bind}$ is defined as the difference between the free energy of the complex and unbound state. All energy terms are calculated by CHARMm and the electrostatics energy is calculated using a Generalized Born implicit solvent model. The total energy is calculated as an empirical weighted sum of van der Waals interactions (E_{vdW}), electrostatic interactions (ΔG_{elec}), an entropy contribution ($-TS_{sc}$) related to the changes in side-chain mobility, and a non-polar, surface dependent, contribution to solvation energy (ΔG_{np}).

This protocol was used to predict the impact of single or a combination of mutations of human residues to their rat counterpart. Finally, the full interaction surface between DN45 and human mGlu4 was scanned.

We also calculated the impact of a single point mutation of each of these interface residues to the overall stability of mGlu4 using the Calculate Mutation Energy Stability protocol (40). It performs combinatorial amino-acid scanning mutagenesis on a set of selected amino-acid residues by mutating each of them to one or more specified amino-acid types. The energy effect of each mutation on the protein stability (mutation energy, $\Delta\Delta G_{mut\text{-}stab}$) is calculated as the difference of the free energy of folding ($\Delta\Delta G_{folding}$) between the mutated structure and the wild type protein: $\Delta\Delta G_{mut\text{-}stab}$ = $\Delta\Delta G_{folding}$(mutant) - $\Delta\Delta G_{folding}$(wild type). The $\Delta\Delta G_{folding}$ is defined as the free energy difference between the folded (ΔG_{fld}) and unfolded (denaturated) states (ΔG_{unf}) of the protein: $\Delta\Delta G_{folding}$ = ΔG_{fld} - ΔG_{unf}. Note that a negative value of $\Delta\Delta G_{mut}$ indicates the mutation has a stabilizing effect, and conversely, a positive value indicates the mutation has a destabilizing effect. The energy of the folded state of the

wild type is derived from the input structure. The structures of the mutants in the folded state are modeled by keeping the backbone rigid while optimizing the side-chains using the ChiRotor algorithm (41). Before evaluating the folding energy terms, the structures of the wild type and mutants are energy minimized using CHARMm. The unfolded state is modeled as a relaxed penta-peptide in an extended conformation with the mutated residue in the center. The peptide model is applied only to the short range interactions involving the mutated residues and it is extended with a Gaussian chain model to account for the long-range electrostatic interactions. This is based on the hypothesis that most of the contacts between amino acid residues in the unfolded protein are only sporadic if the residues are not immediate neighbors along the sequence. Considering that van der Waals interactions decline sharply with distance and contribute only at very close contacts; the method neglects the non-polar interactions between the residues that are separated by more than two peptide bonds in sequence.

All energy terms are calculated by CHARMm, and the electrostatics energy is calculated using a Generalized Born implicit solvent model. The total energy is calculated as an empirical weighted sum of van der Waals (E_{vdW}) interaction, electrostatic interaction (ΔG_{elec}), an entropy contribution ($-TS_{sc}$) related to side-chain mobility, and a non-polar, surface dependent, contribution to solvation energy (ΔG_{np}). The calculations were performed in pH-dependent mode.

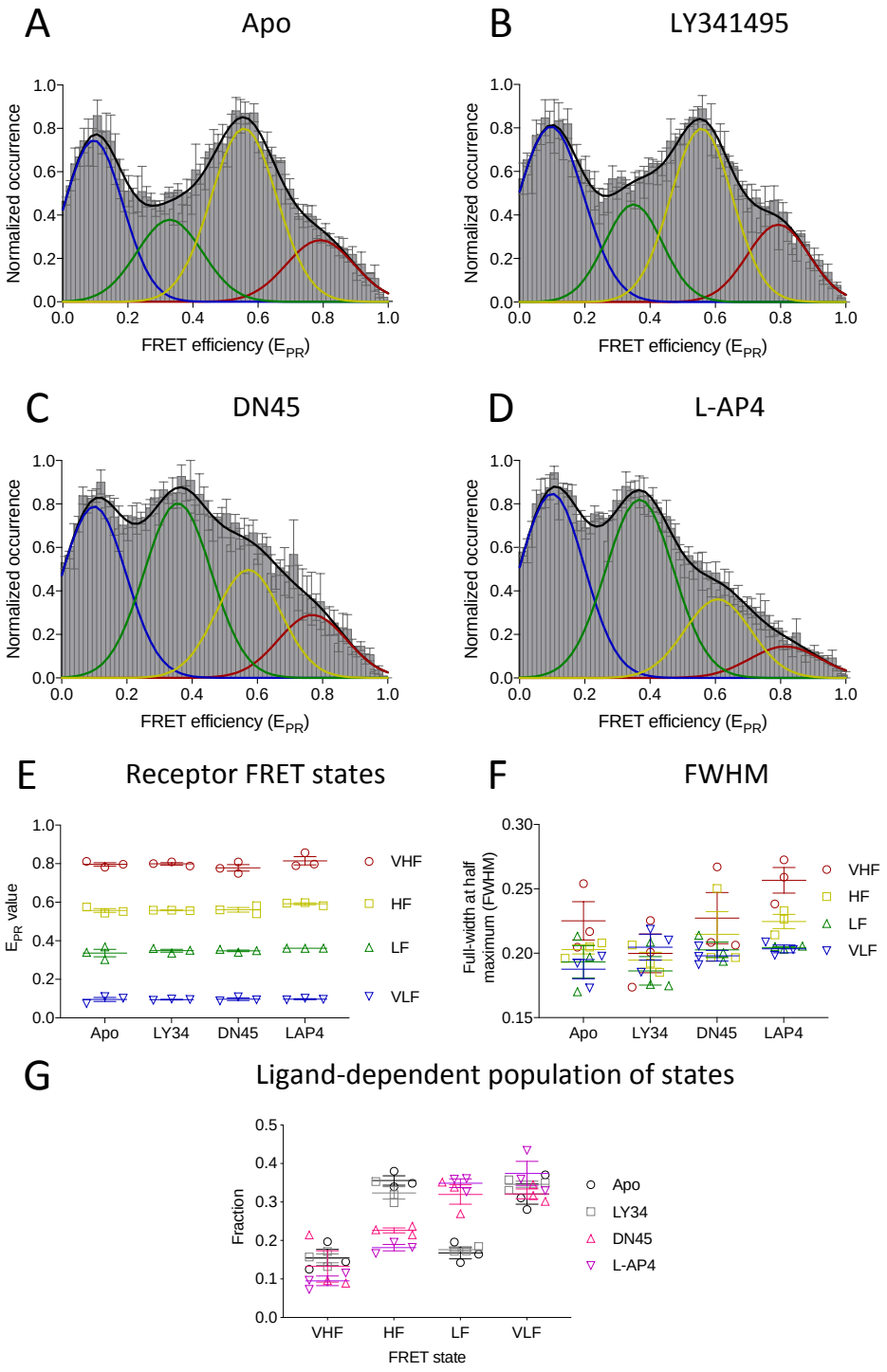

Fig. S1. Agonist action of DN45 nanobody on VFT reorientation analyzed by smFRET. *(A-D)* FRET efficiency histograms of mGlu4 dimers N-terminally SNAP-labeled with BG-Cy3b donor and BG-d2 acceptor fluorophores in the absence of ligand (Apo) or in the presence of DN45, LY341495 or L-AP4. The average global fit (black) as well as the very low FRET (VLF, blue), low FRET (LF, green), high FRET

(HF, yellow) and very high FRET (VHF, red) populations obtained by gaussian fitting using variable E_{PR} and full width half maximum (FWHM) values are shown. E) Mean E_{PR} and F) FWHM values for each of the four states under different ligand conditions. G) Fraction of each of the four states relative to all states under different ligand conditions. The histograms *A*-*D* show the mean number of molecules determined from three independent biological replicates each normalized to the maximum number per replicate with error bars given as SEM. Data of *E*-*G* are represented as mean ± SEM of three independent biological replicates.

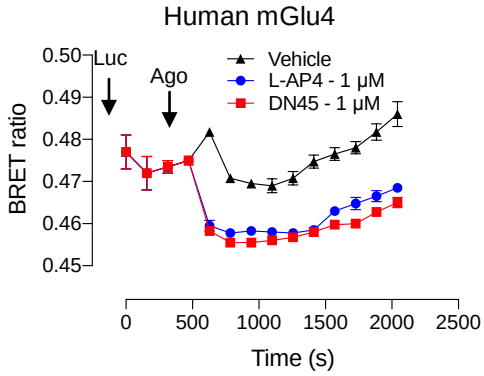

Fig. S2. Gi rearrangement kinetics visualized by change in BRET between Gαi-Rluc and Gγ-Venus. Signals were measured at 530 nm for the Venus and 480 nm for the Rluc. A basal signal was measured for 10 minutes after addition of coelenterazine (Luc). Next, the buffer and agonist conditions were added (Ago).

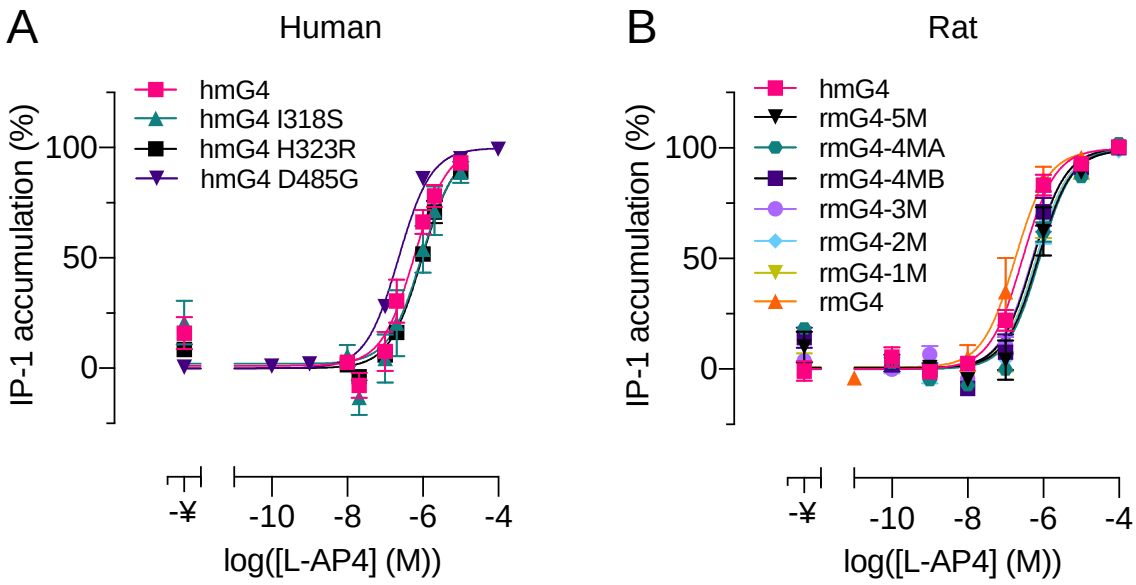

Fig. S3. Activation of human and rat mGlu4 constructs by L-AP4 in IP-1 accumulation assay. *(A)* IP-1 accumulation of human mGlu4 wild-type and mutated receptors. *(B)* IP-1 accumulation of the human and rat mGlu4 wild-type receptors and mutated rat mGlu4 receptors.

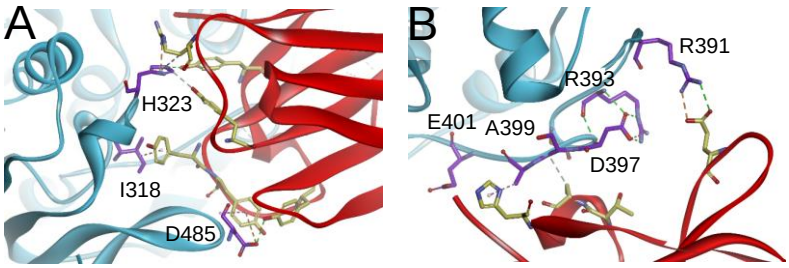

Fig. S4. Key interacting residues in the modelled complex of DN45 with human mGlu4 VFT (Fig. 3A). Residues of DN45 are displayed as yellow sticks, those of mGlu4 VFT in purple. *(A)* Lobe 2 and *(B)* lobe 1 interactions are shown as dashed lines (H-bonds are green, salt bridges are orange, hydrophobic interaction are purple).

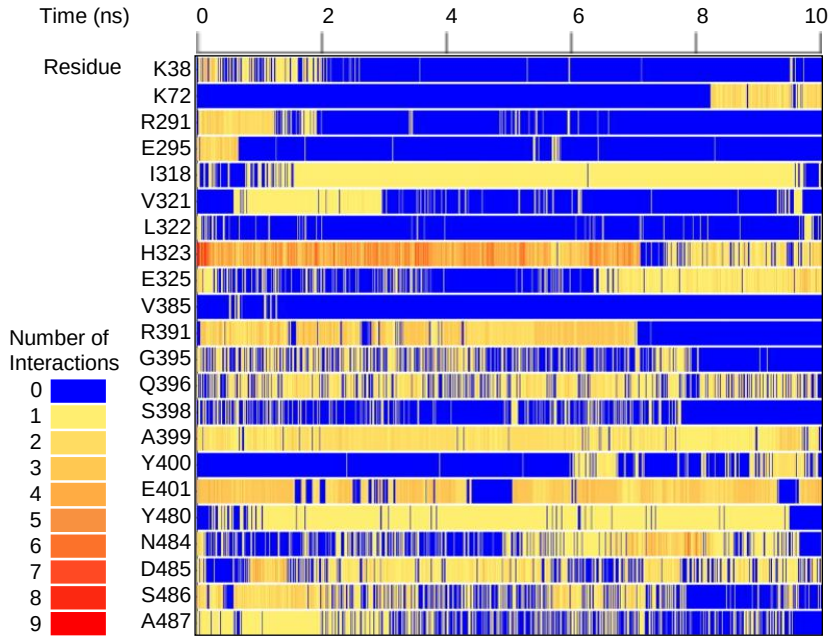

Fig. S5. Non-boned interactions as function of time for 10 ns molecular dynamics simulation of the docked DN45 mGlu4 complex for top interacting residues.

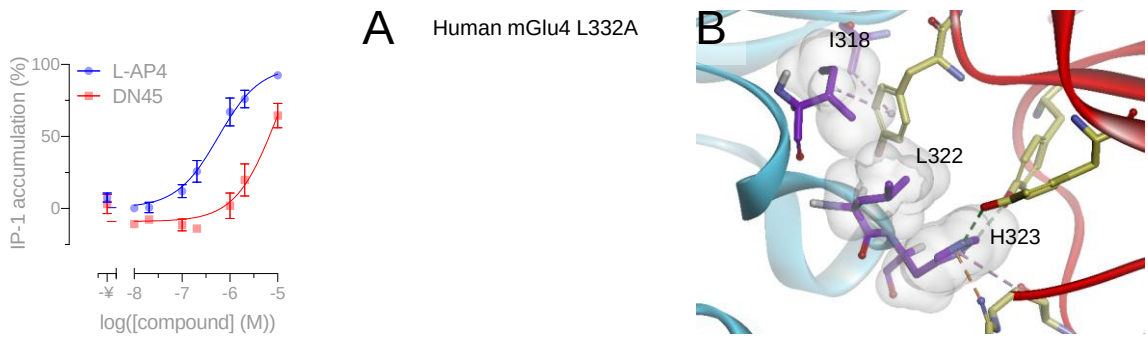

Fig. S6. Role of L322 in stabilizing interactions between the human mGlu4 VFT and DN45. *(A)* IP-1 accumulation induced by L-AP4 and DN45 on a human L322A mutated mGlu4 receptor. *(B)* Expanded view of Fig. 3A around residue L322 in the modelled complex of DN45 and the human mGlu4 VFT. Contacting residues in mGlu4 are displayed with light grey van der Waals surfaces.

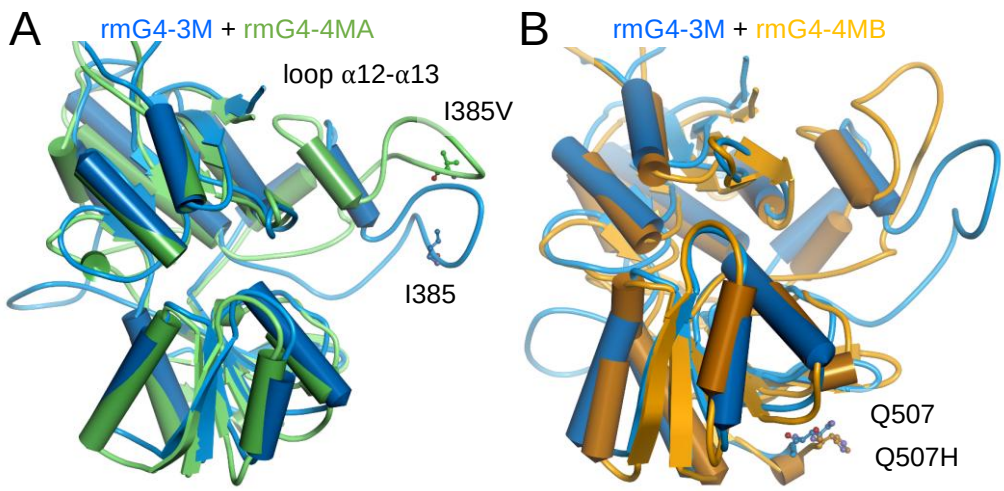

Fig. S7. Superimposition of VFTs of rmG4-3M and rmG4-4MA or rmG4-4MB models after 10 ns molecular dynamics simulation**.** *(A)* Superimposition of rmG4-3M and rmG4-4MA. *(B)* Superimposition of rmG4-3M and rmG4-4MB.

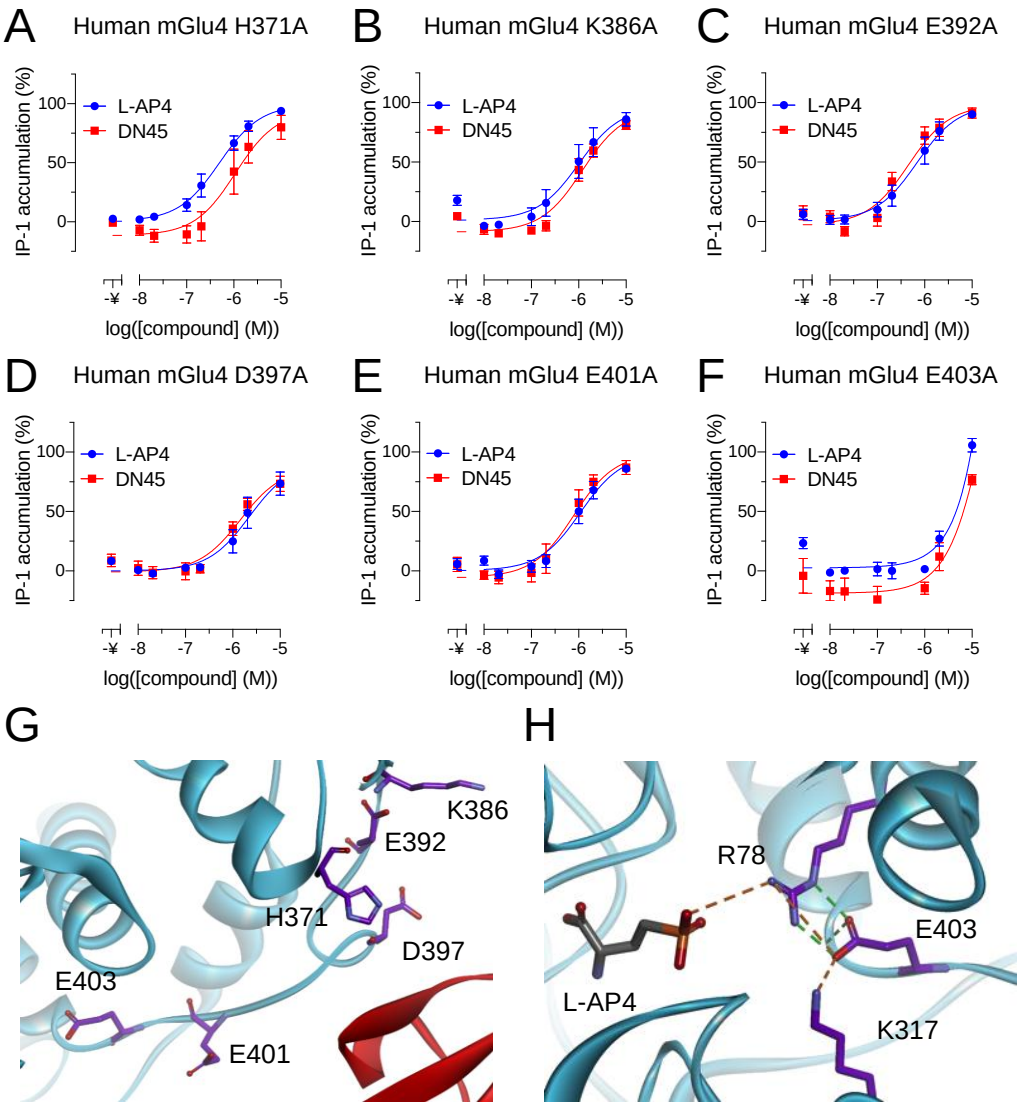

Fig. S8. Effect of alanine mutations on loop of lobe 1 of the human mGlu4 VFT. *(A-F)* Effect on the accumulation of IP-1 induced by L-AP4 and DN45 *(G-H)* 3D location of mutated residues in the modelled complex (Fig. 4). Note that E403 is stabilizing critical residues (R78 and K317) for L-AP4 binding explaining the decreased activation shown in panel F.

Table S1. Affinity (pK_D) and standard error of the mean (SEM) of DN45 for the different mGlu4 constructs. The used statistical analysis is mentioned in the main figure legends and values are compared with the control unless stated otherwise.

Fig.	Receptor	Condition	pKD ± SEM	N	P-value
1D	hmG4	+ 10 µM L-AP4	8.53 ± 0.09	3	-
3B	hmG4	+ 1 µM L-AP4	8.29 ± 0.02	3	Control
	hmG4 I318S	+ 1 µM L-AP4	8.00 ± 0.07	3	0.0168
	hmG4 H323R	+ 1 µM L-AP4	7.60 ± 0.06	3	0.0002
3D	hmG4	+ 1 µM L-AP4	8.28 ± 0.06	5	Control
	rmG4-5M	+ 1 µM L-AP4	7.70 ± 0.11	6	0.4613
	rmG4-4MA	+ 1 µM L-AP4	8.01 ± 0.10	3	0.9801
	rmG4-4MB	+ 1 µM L-AP4	7.93 ± 0.17	3	0.8392
5B	mGlu2-4	+ 10 µM L-AP4	8.34 ± 0.09	5	(L-AP4 vs Glu) = 0.1130
		+ 1 mM Glutamate	8.54 ± 0.10	5	(Glu vs LY37) = 0.0259
		+ 10 µM LY379268	8.14 ± 0.07	3	(LY37 vs L-AP4) = 0.4757

Table S2. Potency (pEC_{50}) and standard error of the mean (SEM) for the different mGlu4 constructs. The used statistical analysis is mentioned in the main figure legends and values are compared with the control.

Fig.	Receptor	Condition	pEC50 ± SEM	N	P-value
2A	hmG4	L-AP4	6.12 ± 0.03	3	Control
		DN45	6.57 ± 0.23	3	0.1222
2C	hmG4	L-AP4	7.22 ± 0.03	3	Control
		DN45	7.22 ± 0.11	3	0.9505
2D	hmG4	L-AP4	6.54 ± 0.10	3	Control
		DN45	6.65 ± 0.21	3	0.6674
		Glutamate	4.59 ± 0.15	3	-
2F	hmG4	L-AP4	6.16 ± 0.18	4	Control
		+ 5 nM DN45	5.96 ± 0.12	4	0.7166
		+ 10 nM DN45	6.19 ± 0.19	4	0.9990
		+ 100 nM DN45	5.74 ± 0.07	3	0.4949
3C	hmG4	DN45	6.63 ± 0.20	3	Control
	hmG4 I318S	DN45	5.68 ± 0.23	3	0.1794
	hmG4 H323R	DN45	5.07 ± 0.54	3	0.0367
3E	hmG4	DN45	6.65 ± 0.21	3	Control
	rmG4-5M	DN45	6.59 ± 0.54	3	0.7939
	rmG4-4MA	DN45	6.59 ± 0.02	3	0.9977
	rmG4-4MB	DN45	6.31 ± 0.08	3	0.7524
4C	hmG4 (A399N/E401S - N-Glycan)	L-AP4	6.05 ± 0.08	3	Control
	rmG4-4MA	DN45	5.18 ± 0.19	3	0.0070
4D	hmG4 (R391M+R393W+A399K)	L-AP4	5.74 ± 0.06	3	-
4E	hmG4 (H371E+R391M+R393W+A399K)	L-AP4	7.00 ± 0.01	3	-
		DN45	6.37 ± 0.06	3	-
4F	hmG4 (H371E+R391M+R393W+A399K)	L-AP4	6.85 ± 0.16	3	Control
		+ DN45	6.33 ± 0.13	3	0.0351
5C	mGlu2-4	+ LY37	6.11 ± 0.19	3	-
5D	mGlu2-4	LY37	6.02 ± 0.14	5	Control
		+ 10 µM DN45	8.49 ± 0.14	4	<0.0001

Table S3. Fraction and standard error of the mean (SEM) for single-molecule FRET analysis. The statistical analysis is mentioned in the main figure legend and values are compared to the control unless stated otherwise.

Fig.	Receptor	Condition	Fraction ± SEM	N	P-value
2B	hmG4	Apo	0.320 ± 0.025	3	Control
		LY34	0.353 ± 0.012	3	0.3263
		DN45	0.584 ± 0.014	3	<0.0001
		L-AP4	0.658 ± 0.005	3	<0.0001
		DN45 v. L-AP4			0.0073

Table S4. Impact on the binding of DN45 to hmGlu4 and overall stability of folding of the complex upon virtual mutation of twelve human residues to corresponding rat residues at the end of 10 ns simulation.

#	Human	Rat	Mutation energy binding (kcal/mol)	Effect	Mutation energy stability (kcal/mol)	Effect
66	P	A	0.07	Neutral	0.54	Destabilizing
224	V	L	-0.04	Neutral	1.22	Destabilizing
245	D	N	0.12	Neutral	0.53	Destabilizing
262	A	T	0.11	Neutral	-0.42	Neutral
270	R	K	0.02	Neutral	0.06	Neutral
280	A	G	0.09	Neutral	1.97	Destabilizing
281	V	I	0.01	Neutral	-0.06	Neutral
385	V	I	0.01	Neutral	-1.23	Stabilizing
507	H	Q	0.01	Neutral	-0.3	Neutral
318	I	S	1.55	Destabilizing	3.14	Destabilizing
323	H	R	2.96	Destabilizing	2.92	Destabilizing
485	D	G	0.69	Destabilizing	0.89	Destabilizing

Table S5. Predicted difference in binding energy of DN45 to rat mGlu4 upon mutation of 5 selected rat residues to corresponding human residues.

#	Rat	Human	Mutation energy binding (kcal/mol)	Effect
385	I	V	0.02	Neutral
507	Q	H	0.02	Neutral
318	S	I	-1.04	Stabilizing
323	R	H	-2.52	Stabilizing
485	G	D	-0.81	Stabilizing

Supplementary Information References

1. K. D. Cromie, G. V. H. and C. Boutton, Nanobodies and their Use in GPCR Drug Discovery. *Curr. Top. Med. Chem.* **15**, 2543–2557 (2015).
2. A. Gupta, *et al.*, Increased Abundance of Opioid Receptor Heteromers Following Chronic Morphine Administration. *Sci. Signal.* **3** (2010).
3. C. J. Hutchings, M. Koglin, W. C. Olson, F. H. Marshall, Opportunities for therapeutic antibodies directed at G-protein- coupled receptors. *Nat. Rev. Drug Discov.* **16**, 787–810 (2017).
4. T. Hino, T. Arakawa, H. Iwanari, T. Yurugi-kobayashi, G protein-coupled receptor inactivation by an allosteric inverse-agonist antibody. *Nature* **482**, 237–240 (2012).
5. A. S. Hauser, M. M. Attwood, M. Rask-Andersen, H. B. Schiöth, D. E. Gloriam, Trends in GPCR drug discovery: New agents, targets and indications. *Nat. Rev. Drug Discov.* **16**, 829–842 (2017).
6. J. Kniazeff, L. Prézeau, P. Rondard, J. Pin, C. Goudet, Dimers and beyond : The functional puzzles of class C GPCRs. *Pharmacol. Ther.* **130**, 9–25 (2011).
7. E. Doumazane, *et al.*, A new approach to analyze cell surface protein complexes reveals specific heterodimeric metabotropic glutamate receptors. *FASEB J.* **25**, 66–77 (2011).
8. J. Lee, *et al.*, Defining the Homo- and Heterodimerization Propensities of Metabotropic Glutamate Receptors. *Cell Rep.* **31**, 107605 (2020).
9. S. Yin, *et al.*, Selective actions of novel allosteric modulators reveal functional heteromers of Metabotropic glutamate receptors in the CNS. *J. Neurosci.* **34**, 79–94 (2014).
10. D. M. Delgado, *et al.*, Pharmacological evidence for a metabotropic glutamate receptor heterodimer in neuronal cells. *Elife* **6**, 1–33 (2017).
11. P. Scholler, *et al.*, Allosteric nanobodies uncover a role of hippocampal mGlu2 receptor homodimers in contextual fear consolidation. *Nat. Commun.* **8**, 1 (2017).
12. D. Charvin, mGlu4 allosteric modulation for treating Parkinson's disease. *Neuropharmacology* **135**, 308–315 (2018).
13. C. M. Niswender, *et al.*, Development and Antiparkinsonian Activity of VU0418506, a Selective Positive Allosteric Modulator of Metabotropic Glutamate Receptor 4 Homomers without Activity at mGlu2/4 Heteromers. *ACS Chem. Neurosci.* **7**, 1201–1211 (2016).
14. P. Gubellini, C. Melon, E. Dale, D. Doller, L. Kerkerian-Le Goff, Distinct effects of mGlu4 receptor positive allosteric modulators at corticostriatal vs. striatopallidal synapses may differentially contribute to their antiparkinsonian action. *Neuropharmacology* **85**, 166–177 (2014).
15. B. Vilar, *et al.*, Alleviating pain hypersensitivity through activation of type 4 metabotropic glutamate receptor. *J. Neurosci.* **33**, 18951–18965 (2013).
16. C. Zussy, *et al.*, Dynamic modulation of inflammatory pain-related affective and sensory symptoms by optical control of amygdala metabotropic glutamate receptor 4. *Mol. Psychiatry* **23**, 509–520 (2018).
17. K. Even-Desrumeaux, *et al.*, Masked selection: A straightforward and flexible approach for the selection of binders against specific epitopes and differentially expressed proteins by phage display. *Mol. Cell. Proteomics* **13**, 653–665 (2014).
18. P. Scholler, *et al.*, HTS-compatible FRET-based conformational sensors clarify

membrane receptor activation. *Nat. Chem. Biol.* **13**, 372–380 (2017).
19. R. Chen, L. Li, Z. Weng, ZDOCK : An Initial-Stage Protein-Docking Algorithm. *PROTEIN Struct. Funct. Genet.* **52**, 80–87 (2003).
20. B. Pierce, Z. Weng, ZRANK: Reranking Protein Docking Predictions With an Optimized Energy Function. *PROTEIN Struct. Funct. Genet.* **67**, 1078–1086 (2007).
21. J. Kniazeff, *et al.*, Closed state of both binding domains of homodimeric mGlu receptors is required for full activity. *Nat. Struct. Mol. Biol.* **11**, 706–713 (2004).
22. S. Urwyler, Allosteric modulation of family C G-protein-coupled receptors: from molecular insights to therapeutic perspectives. *Pharmacol. Rev.* **63**, 59–126 (2011).
23. I. Sebastianutto, M. A. Cenci, mGlu receptors in the treatment of Parkinson ' s disease and L-DOPA-induced dyskinesia. *Curr. Opin. Pharmacol.* **38**, 81–89 (2018).
24. S. Duggan, Caplacizumab : First Global Approval. *Drugs* **78**, 1639–1642 (2018).
25. T. Li, *et al.*, Cell-penetrating anti-GFAP VHH and corresponding fluorescent fusion protein VHH-GFP spontaneously cross the blood-brain barrier and specifically recognize astrocytes: Application to brain imaging. *FASEB J.* **26**, 3969–3979 (2012).
26. S. Low, *et al.*, VHH antibody targeting the chemokine receptor CX3CR1 inhibits progression of atherosclerosis. *MAbs* **12**, 1–12 (2020).
27. C. McMahon, *et al.*, Synthetic nanobodies as angiotensin receptor blockers. *Proc. Natl. Acad. Sci. U. S. A.* **117**, 20284–20291 (2020).
28. A. Koehl, *et al.*, Structural insights into the activation of metabotropic glutamate receptors. *Nature* **566**, 79–84 (2019).
29. J. Levitz, *et al.*, Mechanism of Assembly and Cooperativity of Homomeric and Heteromeric Metabotropic Glutamate Receptors. *Neuron* **92**, 143–159 (2016).
30. J. Liu, *et al.*, Allosteric control of an asymmetric transduction in a G protein-coupled receptor heterodimer. *Elife* **6**, 1–19 (2017).
31. T. Galvez, *et al.*, Allosteric interactions between GB1 and GB2 subunits are required for optimal $GABA_B$ receptor function. *EMBO J.* **20**, 2152–2159 (2001).
32. I. Brabet, M. Parmentier, C. De Colle, Comparative effect of L -CCG-I , DCG-IV and k -carboxy- L -glutamate on all cloned metabotropic glutamate receptor subtypes. *Neuropharmacology* **37**, 1043–1051 (1998).
33. P. Scholler, *et al.*, HTS-compatible FRET-based conformational sensors clarify membrane receptor activation. *Nat. Chem. Biol.* **13**, 372–380 (2017).
34. A. Cao, R. B. Quast, F. Fatemi, P. Rondard, Allosteric modulators enhance agonist efficacy by increasing the residence time of a GPCR in the active state. *bioRxiv*, 1–37 (2021).
35. L. Olofsson, *et al.*, Fine tuning of sub-millisecond conformational dynamics controls metabotropic glutamate receptors agonist efficacy. *Nat. Commun.* **5** (2014).
36. A. Sali, T. L. Blundell, Comparative Protein Modelling by Satisfaction of Spatial Restraints. *J. Mol. Biol.* **234**, 779–815 (1993).
37. M. Shen, A. Sali, Statistical potential for assessment and prediction of protein structures. *Protein Sci.* **15**, 2507–2524 (2006).
38. J. C. Phillips, *et al.*, Scalable Molecular Dynamics with NAMD. *J. Comput. Chem.* **26**, 1781–1802 (2005).
39. V. Z. Spassov, L. Yan, pH-Selective mutagenesis of protein–protein interfaces:

In silico design of therapeutic antibodies with prolonged half-life. *PROTEINS Struct. Funct. Bioinforma.* **81**, 704–714 (2012).
40. V. Z. Spassov, L. Yan, A pH-dependent computational approach to the effect of mutations on protein stability. *J. Comput. Chem.* **37**, 2573–2587 (2016).
41. V. Z. Spassov, L. Yan, P. K. Flook, The dominant role of side-chain backbone interactions in structural realization of amino acid code. ChiRotor: A side-chain prediction algorithm based on side-chain backbone interactions. *Protein Sci.* **16**, 494–506 (2007).